954668

OCEAN DATA SYSTEMS, INC.

(NASA-CR-157331) ATMOSPHERIC MODEL DEVELOPMENT IN SUPPORT OF SEASAT. VOLUME 5: TEST RESULTS WITH FINE-MESH (187 BY 187 BY 10) MODEL Final Technical Report (Ocean Data Systems, Inc.) 73 p HC A04/MF A01

N78-28583

Unclas

G3/43 25959

odsi

OCEAN DATA SYSTEMS, INC.
2400 GARDEN ROAD, MONTEREY, CALIFORNIA 93940 • 408/649-1133

Submitted to
JET PROPULSION LABORATORY
Pasadena, California

ATMOSPHERIC MODEL DEVELOPMENT

IN SUPPORT OF SEASAT

VOLUME V - TEST RESULTS WITH FINE-MESH (187x187x10) MODEL

Final Technical Report

Prepared under
JPL Contract Number 954668
(Subcontract of NASA Contract Number NAS7-100)

September 30, 1977

Prepared by
Philip G. Kesel
OCEAN DATA SYSTEMS, INC.
Monterey, California

EXECUTIVE SUMMARY

This Final Report (in five volumes) was prepared by Ocean Data Systems, Inc. for the Jet Propulsion Laboratory under Contract No. 954668 (as amended) in support of the SEASAT Program.

The main objective was to develop atmospheric analysis and prediction models of varying grid resolution, and to test the models using real observational data for the purpose of assessing the impact of grid resolution on short-range numerical weather prediction. The work statement was amended to include a fourth and most highly-resolved model version, which is the subject of this volume.

Model PEFHFV (187 x 187 grid with ten layers) was used to produce a 24-hour forecast using initial conditions for 1200Z, 20 May 1976. This forecast (Run T9) has been compared to its five-layer counterpart on the 187 x 187 grid (Run F24), and to its 63 x 63 coarse-mesh counterpart having the same number of layers (Run T5).

Increases in horizontal resolution are computationally expensive, but lead to significant differences in a one-day forecast. Many of these differences represent improvements. We refer to: (1) improved phase speeds of systems; (2) better

specification of horizontal gradients; (2) the provision for treating smaller (additional) scales; (4) reduction of harmful effects of "computational devices" using coarse-mesh grids. Some of the differences cannot be evaluated on the basis of this small sample of forecasts. We refer to: (1) the prediction of maritime cyclones; (2) precipitation amounts; (3) model energetics; and (4) maintenance of general circulation.

Increases in vertical resolution tend to produce smaller impacts on the forecast, except in the region near and above the tropopause. The effect on forecast precipitation is in the 10-20% range, as opposed to the 100% for increases in the horizontal resolution. There was little or no impact on either the intensities or displacements of extratropical low-pressure centers.

With respect to model energetics (kinetic energy; square vorticity; square divergence), the models tend to "group" according to horizontal resolution. That is to say, the forecasts from the 63 x 63 models looked alike and the forecasts from the 187 x 187 models looked alike -- but the two groups looked different. Finally, the time variations of these parameters show that dynamic initialization is needed to: (1) minimize initialization shock; and (2) stabilize the model context to prevent "wash-out" of small-scale information during the adjustment period (first 6-12 forecast hours).

The corresponding 187 x 187 x 10 model run for Scenario A was not included in this report because it was initialized (by mistake) with a superseded version of the analyses.

TABLE OF CONTENTS

LIST OF TABLES

LIST OF CHARTS

LIST OF CHARTS (Continued)

LIST OF FIGURES

Figure

LIST OF FIGURES (Continued)

I. INTRODUCTION

This is the Final Report of Ocean Data Systems, Inc. (ODSI) prepared for the Jet Propulsion Laboratory (JPL) under Contract No. 954668 (as amended) in support of the SEASAT Program of the National Aeronautics and Space Administration.

The Final Report consists of five volumes. Volume I is the Summary of Findings for modeling activities defined in the original work statement. Volumes II and III contain detailed descriptions of the analysis and prediction models, respectively. Volume IV describes sensitivity studies performed with one version of the prediction model. Volume V summarizes the results obtained with the 187 x 187 x ten-layer prediction model.

IMPORTANT NOTE

Run T10 (Scenario A, 187 x 187 x 10-level model version) was inadvertently initialized with an incorrect, superseded version of the 1200Z, 22 April 1976 analyses. There was not enough computer time available GFE to re-run this forefast.

Table I-1 contains the model descriptors and forecast run numbers which will be used herein. Several classes of

TABLE I-1: DESCRIPTORS AND RUN NUMBERS FOR SCENARIO B FORECASTS.

ITEM	GRID	
	63 x 63	187 x 187
FIVE-LAYER MODELS		
-- DESCRIPTOR	PECHCV	PEFHCV
-- RUN NUMBER	F19	F24
TEN-LAYER MODELS		
-- DESCRIPTOR	PECHFV	PEFHFV
-- RUN NUMBER	T5	T9

exhibits are provided: (1) forecast charts; (2) forecast change charts; (3) forecast error charts; (4) forecast difference charts; and (5) statistical and graphical information describing model performance and model behavior.

Section II contains the test results obtained with model version PEFHFV using initial conditions for 1200Z, 20 May 1976 (Run T9). Resolution effects are discussed in Section III. Comparative performance data are provided to facilitate the evaluation of all forecasts made in Scenario B. Section IV contains the summary and conclusions.

II. TEST RESULTS WITH FINE-MESH MODEL PEFHFV

Model PEFHFV (187 x 187 x 10 levels) was used to produce a 24-hour forecast from 1200Z, 20 May 1976 (Run Number T9). This forecast can be compared to its five-layer counterpart (Run F24) for the 187 x 187 grid, or to its coarse-mesh (63 x 63) counterpart (Run T5) which also has ten levels.

A. Forecast Discussion (Run T9)

Chart VI-5 contains the 24-hour sea-level pressure forecast valid at 1200Z, 21 May 1976. Of the six major low-pressure centers being evaluated, the algebraic average error of these centers was -2.7 millibars. Most of these lows were predicted quite well, but the 972-millibar low near Manchuria was too deep by 16 millibars. Chart VI-1 contains the verification analysis. Other aspects of the forecast were not handled as well as these low centers. There is a spurious low center predicted over the Atlas Mountains in northwestern Africa, for example. In addition, the subtropical ridge was not handled well in the Pacific area.

Chart VI-8 contains the forecast changes at sea level. The contour interval is 4 MBS. Chart VI-3 contains the actual pressure changes. The area of major disagreement is in the Pacific area. Chart VI-10 contains the forecast error pattern. This shows that the Atlas Mountain low was in error by 12 MBS, the low near Manchuria was in error by 16 MBS, and the Pacific area was in error by 4-12 MBS, generally. North America looked quite good, on the other hand.

Chart VI-6 contains the 24-hour 500 MB height forecast valid at 1200Z, 21 May 1976. The pattern has a smooth appearance, but not excessively so. Chart VI-2 contains the verification analysis. Chart VI-9 contains the forecast changes. The 240-meter fall center near Manchuria is the most significant change center. The centers south of Iceland and over England are also significant centers. Chart VI-4 shows the actual changes at 500 MBS. Except for the Pacific area, the agreement is quite good. Chart VI-11 shows the forecast error pattern. There are large areas over which the 500 MB forecast was quite good.

The 500 MB temperature forecast is provided as Chart VI-7. This looks quite smooth, except for portions of the subtropics. Temperature/height falls over the central Pacific were excessive.

Table V-9 contains a statistical summary for Run T9. The RMS forecast changes were too large compared to actual changes at both sea level and 500 MBS. The forecast errors indicate that the forecast ran out of skill (compared to persistence) after one day, but considerable skill remains over large areas in the middle and high latitudes, as was seen in the chart discussion.

B. Comparative Performance Data

Table V-1 contains the sea-level pressure forecasts (central pressures) for six extratropical lows by four models of differing resolution. The two fine-mesh (187 x 187 grid) models (Run F24 and Run T9) deepened the lows about 2.7 MBS too much on the average. Not all of the lows were affected by resolution differences, however. The coarse-mesh models (Run F19 and Run T5) did better on the average. Table V-6 contains the predicted precipitation amounts from these four model versions. It shows quite clearly that the 187 x 187 models precipitated double the amounts precipitated by the 63 x 63 models. This accounts for the 2.7-MB average central pressure difference.

Table V-2 contains performance statistics for the four models at 500 MBS. Run T9 predicted more change than the other models. The forecast errors, however, were quite comparable at 500 MBS. Table V-3 contains performance statistics at sea level. At sea level, there is a greater difference between the various models than at 500 MBS.

1. Kinetic Energy (KE)

Figure VII-1 shows the layer-mean kinetic energy forecast change (level by level), expressed in percent, for four model versions. The fine-mesh versions, PEFHCV and PEFHFV, produced comparable results; the coarse-mesh versions, PECHCV and PECHFV produced comparable results. But, the two groups are quite dissimilar. The coarse-mesh models tended to lose KE, while the fine-mesh models either gained KE or had smaller losses. Table V-7 contains the actual ΔKE values which were used to construct Figure VII-1. At Sigma=0.3 level, the level of maximum wind, the coarse-mesh models lost about 25% of the initial KE, while the fine-mesh models only lost about half as much.

Figures VII-2 through VII-5 contain forecast kinetic energy cross-sections (latitude vs. sigma level) for the four forecasts. It is difficult to detect the jet-core magnitude difference between the coarse-mesh and fine-mesh models by examining these diagrams. The 1-2 unit difference shows up as a dashed, intermediate contour at the jet core for Runs F24 and T9.

Figures VII-6 through VII-10 contain the kinetic energy (forecast) time variations (for four model versions) at the five model levels, respectively. Except at the

Sigma=0.1 level, horizontal resolution is clearly the dominant influence. At Sigma=0.1 (above the tropopause, generally), the vertical resolution is dominant.

2. Square Vorticity (SV)

Figure VII-11 shows the layer-mean square vorticity (SV) forecast change (expressed in percent) for each of four model versions. Once again, the results tend to group according to horizontal resolution, except at the Sigma=0.1 level. Clearly, the fine-mesh models tend to predict larger increases (smaller decreases) in SV than the coarse-mesh models. Table V-8 contains the actual ΔSV values which were used to construct Figure VII-11. Note also that within each horizontal resolution, the coarse-vertical resolution models tend to predict larger increases (smaller decreases) in SV than the fine-vertical models.

Figures VII-12 through VII-16 contain the square vorticity (forecast) time variations at five sigma levels, respectively. This also shows the strong tendency to group according to horizontal resolution. The exception, once again, is at Sigma=0.1 level. The coarse-mesh models tend to lose SV from the outset of the forecast. The fine-mesh models gain SV in the first 6-12 hours at the lowest level, with compensating losses at high levels.

3. Square Divergence (SDIV)

Figures VII-17 through VII-21 show the time variations of square divergence (SDIV) at each of five sigma levels, respectively. Once again, the results tend to group according to horizontal resolution. Runs F24 and T9 show larger increases in SDIV, especially in the early forecast hours.

III. RESOLUTION EFFECTS SUMMARY

Difference charts and statistical information will be provided and discussed in order to demonstrate the variations in short-range forecasts caused by changes in the horizontal and/or vertical resolution.

A. Horizontal Resolution

Charts VI-12 and VI-13 show the difference between Run T9 (187 x 187 x 10) and Run T5 (63 x 63 x 10) at sea level and at 500 MBS, respectively. On Chart VI-12, the differences range from -7.2 MBS to +3.3 MBS. Table V-5, Part B, shows the RMS pressure difference to be 1.4 MBS. On Chart VI-13, the differences range from -66 meters to +50 meters. The contour interval on these charts is 2 MBS and 15 meters, respectively. The differences pattern well, and tend to be in meteorological scales.

In Table V-5, we also provide the difference statistics for the five-layer model versions. Note that the ranges of differences (-9.6 MBS to +4.5 MBS, and -69.6 meters to +61.0 meters) are larger in the five-layer models than in the ten-layer models. At sea level, the RMS difference is also larger in the five-layer case.

B. Vertical Resolution

Charts VI-14 and VI-15 contain the differences between Run T9 (187 x 187 x 10) and Run F22 (187 x 187 x 5) at sea level and 500 MBS, respectively. At sea level, the differences range from -3.2 MBS to +7.8 MBS. At 500 MBS, the differences range from -37.9 meters to +35.0 meters. These patterns appear to be smaller in horizontal scale size than those presented in Charts VI-12 and VI-13, earlier.

Table V-4 contains statistical information about the differences arising from doubling the vertical resolution for each horizontal resolution. On the 187 x 187 grid, the RMS difference is greater (0.95 versus 0.76 MBS at sea level, and 9.10 versus 7.27 meters at 500 MBS). The increased ranges of differences support this statement.

Finally, the reader should compare Tables V-4 and V-5. Note that the RMS differences due to horizontal mesh increases tend to be larger than the RMS differences due to vertical resolution increases, but in a proportional manner. Recall that we tripled the horizontal resolution but doubled the vertical resolution.

IV. CONCLUSIONS AND RECOMMENDATIONS

In this volume, we have presented test results obtained from execution of the fine-mesh model PEFHFV (187 x 187 x ten levels) using real initial conditions for Scenario B (1200Z, 20 May 1976).

Increases in horizontal resolution are computationally expensive, but certain benefits are realized: (1) more realistic phase speeds of troughs/fronts; (2) better representation of horizontal gradients; (3) the provision for treating smaller scales; (4) the reduction of harmful effects of computational devices; (5) the scale of dissipation becomes further removed from the scales producing eddy kinetic energy; (6) the effects of parameterized convection are not smeared upscale as much; (7) sharp increases (100%) in precipitation; and (8) improved maintenance of mean zonal flow.

Increases in vertical resolution tend to produce smaller impacts on the forecasts. The effect on precipitation is in the 10-20% range. There was little or no impact on either the intensity or displacement of sea-level pressure systems. At higher altitudes, the ten-layer models allowed for improved specification of winds and temperatures (especially near the tropopause).

Once again, it was evident that dynamic initialization is needed: (1) to minimize initialization shock; (2) improve model energetics; and (3) stabilize the model context to prevent "wash-out" of small-scale information (such as SEASAT data).

Since only one 187 x 187 x 10 model run was completed (using the same initial state as other model versions), we regard the results pertaining to Run T9 as being tentative. This work should be extended to other data cases, with and without dynamic initialization. No engineering adjustments could be made to the fine-mesh models, since there was not enough GFE computer support to permit the necessary test runs. Clearly, the expertise developed as a consequence of the sensitivity studies (reported on in Volume IV) could and should be exploited.

V. TABLES

TABLE V-1: 24-HOUR FORECAST CENTRAL PRESSURES* (MBS) USING FOUR MODELS OF DIFFERING RESOLUTION. SCENARIO B.

MODEL	RUN	LOW-PRESSURE CENTERS						AVERAGE ALGEBRAIC ERROR (MBS)
		CHINA	EAST OF KAMCHATKA	ALASKAN GULF	MAINE	CENTRAL ATLANTIC	ICELAND-ENGLAND	
PEFHCV	F24	975	992	1007	1002	1001	1000	-2.8
PECHCV	F19	978	995	1008	1004	1005	1000	-0.7
PEFHFV	T9	972	992	1007	1003	1005	999	-2.7
PECHFV	T5	978	996	1007	1006	1007	1000	0.0
STARTING ANALYSIS		988	988	1003	1001	1009	1004	
VERIFICATION ANALYSIS		988	992	1008	1004	1006	996	

* FROM 1200Z, 20 MAY 1976

TABLE V-2: PERFORMANCE STATISTICS FOR FOUR FORECAST MODELS OF DIFFERING RESOLUTION: 500MB HEIGHTS. SCENARIO B.

RMS DIFFERENCES (METERS)

SCENARIO	RUN	MODEL	24-HOUR			48-HOUR		
			ACTUAL CHANGE	FORECAST CHANGE	ERROR	ACTUAL CHANGE	FORECAST CHANGE	ERROR
B	T9	PEFHFV	38.6	43.7	38.1	52.3	--	--
	F19	PECHCV	38.6	35.4	39.3	52.3	52.2	50.8
	T5	PECHFV	38.6	35.0	38.0	52.3	52.7	50.4
	F24	PEFHCV	38.6	36.5	38.2	52.3	--	--

TABLE V-3: PERFORMANCE STATISTICS FOR FOUR FORECAST MODELS OF DIFFERING RESOLUTION: SEA-LEVEL PRESSURE. SCENARIO B.

RMS DIFFERENCES (MBS)

SCENARIO	RUN	MODEL	24-HOUR			48-HOUR		
			ACTUAL CHANGE	FORECAST CHANGE	ERROR	ACTUAL CHANGE	FORECAST CHANGE	ERROR
B	T9	PEFHFV	3.34	3.70	3.70	4.35	--	--
	F19	PECHCV	3.34	3.14	3.55	4.35	4.27	3.83
	T5	PECHFV	3.34	2.99	3.34	4.35	4.18	3.70
	F24	PEFHCV	3.34	3.66	3.89	4.35	--	--

TABLE V-4: DIFFERENCE STATISTICS: SCENARIO B
TEN-LAYER FORECAST MINUS FIVE-
LAYER FORECAST.

A. COARSE-MESH MODELS (T5 - F19).

PARAMETER	DIFFERENCE STATISTICS			
	RMS	MEAN	MAX	MIN
SEA-LEVEL PRESSURE (MBS)	0.76	0.14	4.88	-2.50
500MB HEIGHT (METERS)	7.27	-1.12	28.3	-23.4

B. FINE-MESH MODELS (T9 - F24).

PARAMETER	DIFFERENCE STATISTICS			
	RMS	MEAN	MAX	MIN
SEA-LEVEL PRESSURE (MBS)	0.95	0.06	7.76	-3.22
500MB HEIGHT (METERS)	9.10	-3.16	35.0	-37.9

TABLE V-5: DIFFERENCE STATISTICS: SCENARIO B
FINE-MESH FORECAST MINUS COARSE-MESH FORECAST.

A. FIVE-LAYER MODELS (F24 - F19).

PARAMETER	DIFFERENCE STATISTICS			
	RMS	MEAN	MAX	MIN
SEA-LEVEL PRESSURE (MBS)	1.58	-0.68	4.50	-9.6
500MB HEIGHT (METERS)	9.8	-0.44	61.0	-69.6

B. TEN-LAYER MODELS (T9 - T5).

PARAMETER	DIFFERENCE STATISTICS			
	RMS	MEAN	MAX	MIN
SEA-LEVEL PRESSURE (MBS)	1.40	-0.75	3.28	-7.24
500MB HEIGHT (METERS)	10.3	-2.47	49.6	-66.1

TABLE V-6: THE EFFECT OF (FORECAST) MODEL RESOLUTION ON PRECIPITATION. SCENARIO B.

		AVERAGE PRECIPITATION PER GRID POINT*			
MODEL		PEFHFV	PECHCV	PECHFV	PEFHCV
RUN IDENT		T9	F19	T5	F24
	6	.043	.033	.030	.043
	12	.081	.057	.050	.096
	18	.116	.076	.066	.148
FORECAST	24	.154	.098	.082	.205
HOUR	30	-	.116	.097	-
	36	-	.135	.114	-
	42	-	.151	.129	-
	48	-	.169	.144	-

* CUMULATIVE AMOUNTS, IN CENTIMETERS

TABLE V-7: KINETIC ENERGY 24-HOUR FORECAST CHANGES, BY MODEL LEVEL, FOR MODELS OF VARYING RESOLUTION (GIVEN IN PERCENT). SCENARIO B.

	SIGMA LEVEL				
MODEL	0.9	0.7	0.5	0.3	0.1
PEFHFV (T9)	14.0	-5.4	-6.4	-11.6	-24.9
PECHCV (F19)	-13.7	-27.6	-23.7	-23.5	-29.4
PECHFV (T5)	-23.3	-30.6	-26.8	-24.9	-19.3
PEFHCV (F24)	27.8	-3.2	-6.6	-15.2	-22.2

TABLE V-8: SQUARE VORTICITY 24-HOUR FORECAST CHANGES, BY MODEL LEVEL, FOR MODELS OF VARYING RESOLUTION (GIVEN IN PERCENT). SCENARIO B.

	SIGMA LEVEL				
MODEL	0.9	0.7	0.5	0.3	0.1
PEFHFV (T9)	42.4	-13.9	-11.0	-11.3	-33.6
PECHCV (F19)	-13.9	-48.1	-46.1	-36.6	-43.1
PECHFV (T5)	-31.6	-52.3	-50.3	-40.1	-28.0
PEFHCV (F24)	115.7	12.8	-1.6	-13.9	-25.6

TABLE V-9: MODEL STATISTICS. RUN T9. SCENARIO B.

HOUR	TYPE	DIFFERENCE STATISTICS			
		RMS	MEAN	MAX	MIN
A. SEA-LEVEL PRESSURE (MBS)					
24	FORECAST CHANGE	4.13	-1.07	14.0	-19.1
	ACTUAL CHANGE	3.34	-0.07	17.8	-17.9
	FORECAST ERROR	3.70	-1.00	19.0	-18.5
B. 500-MB HEIGHT (METERS)					
24	FORECAST CHANGE	43.7	-18.9	138.0	-275.0
	ACTUAL CHANGE	38.6	-1.50	201.0	-224.0
	FORECAST ERROR	38.1	-17.4	167.0	-144.0

VI. CHARTS

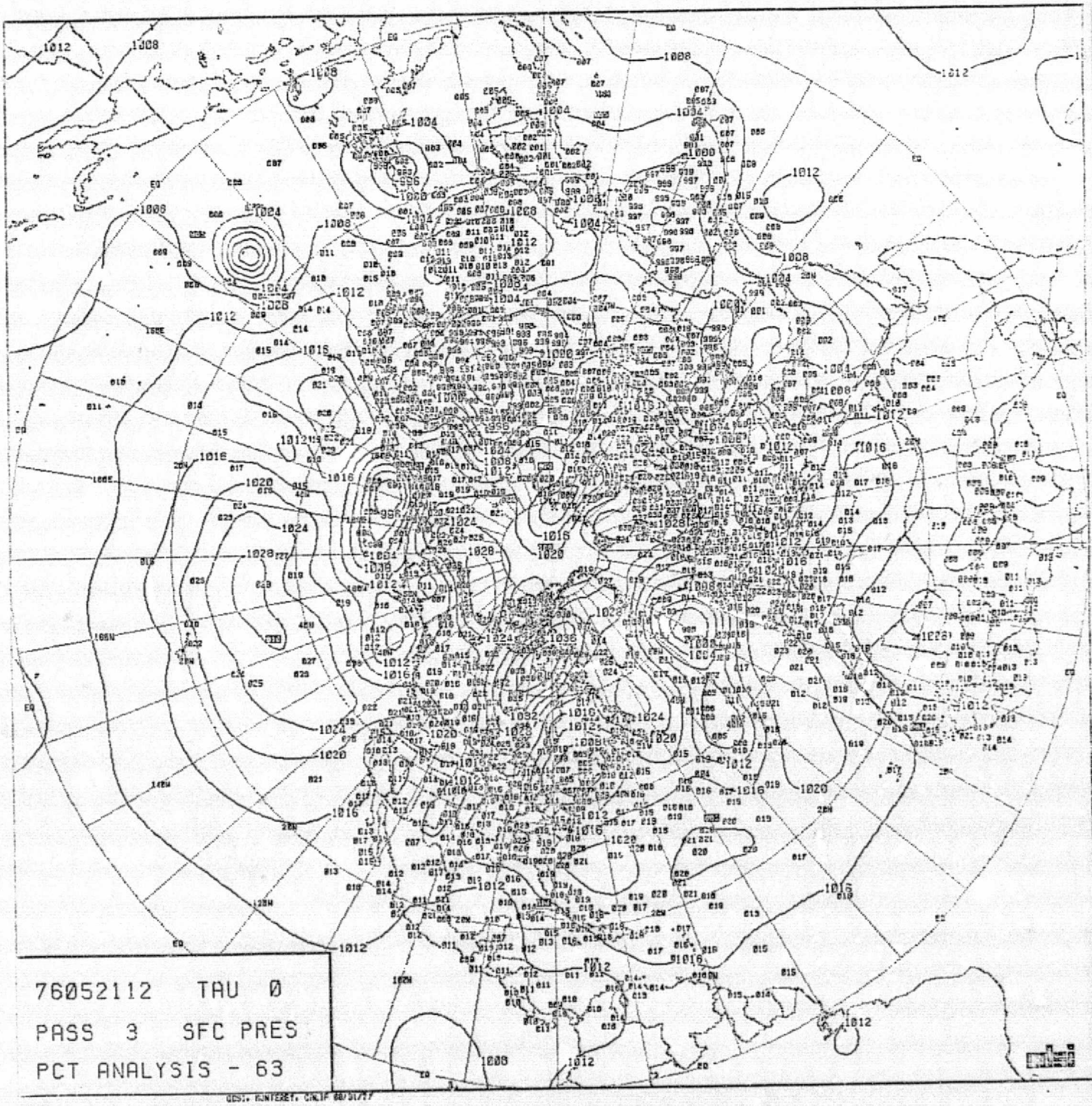

CHART VI-1: SEA-LEVEL PRESSURE ANALYSIS, 1200Z, 21 MAY 1976.

ORIGINAL PAGE IS OF POOR QUALITY

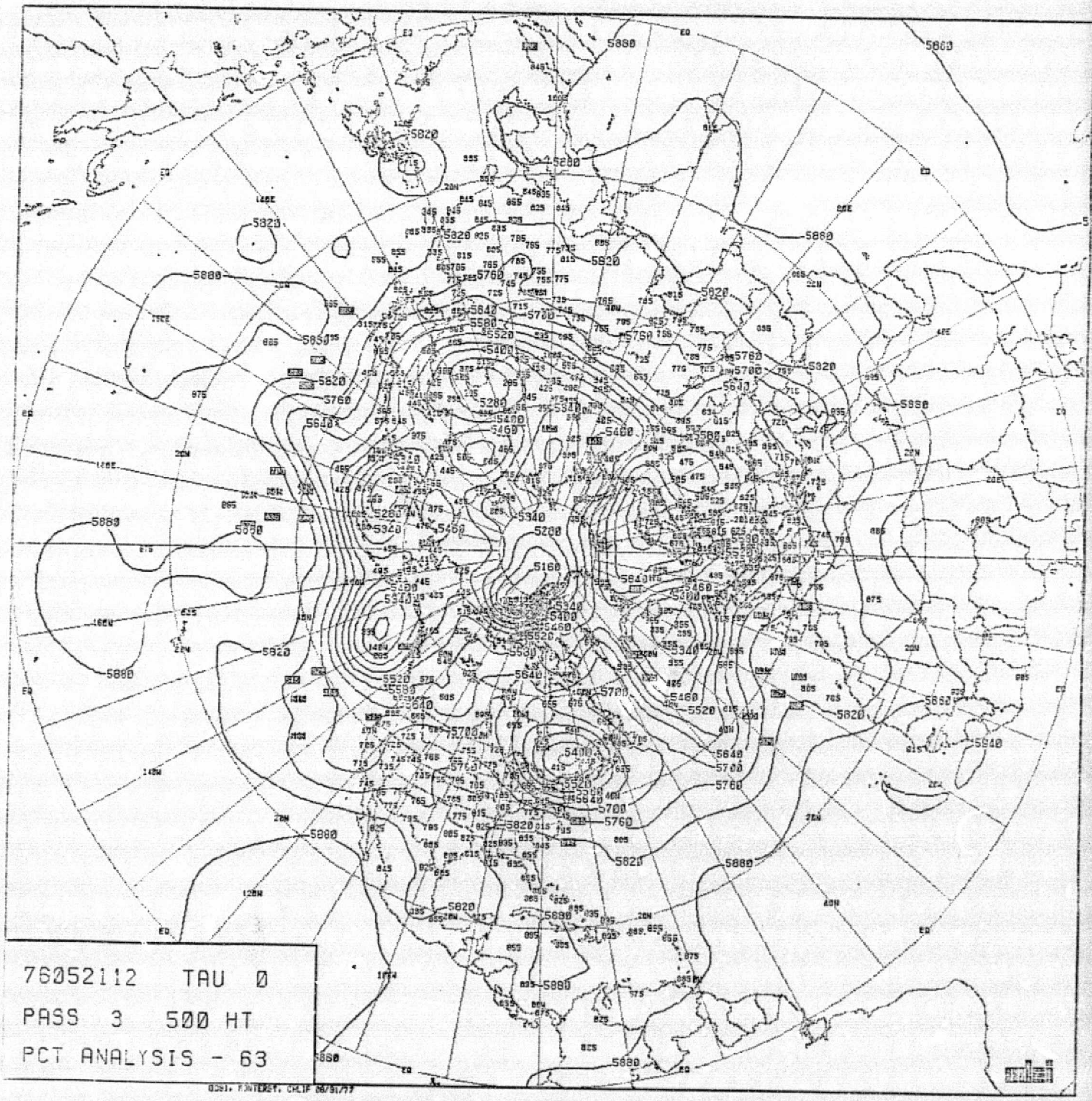

CHART VI-2: 500MB HEIGHT ANALYSIS, 1200Z, 21 MAY 1976.

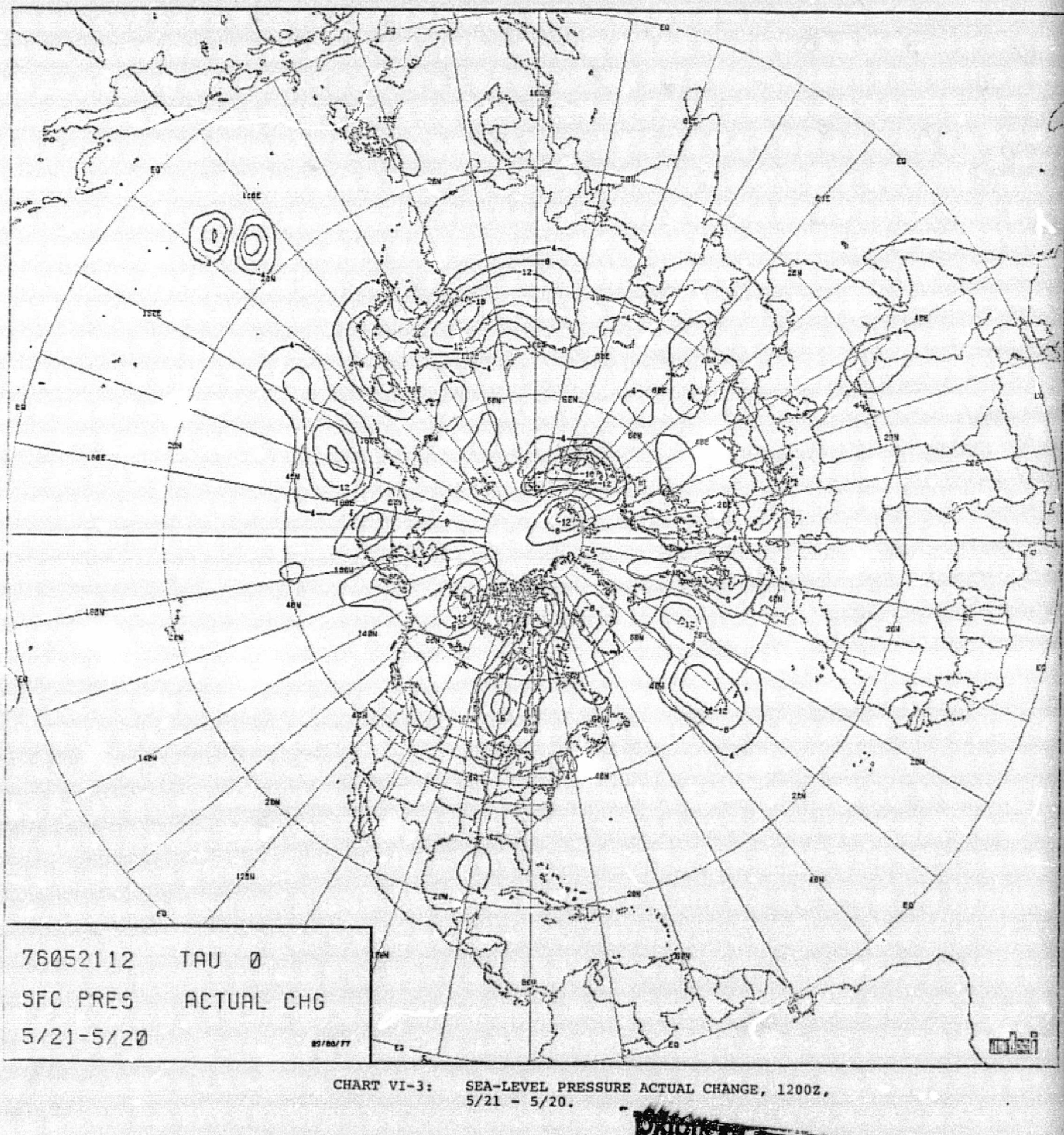

CHART VI-3: SEA-LEVEL PRESSURE ACTUAL CHANGE, 1200Z, 5/21 - 5/20.

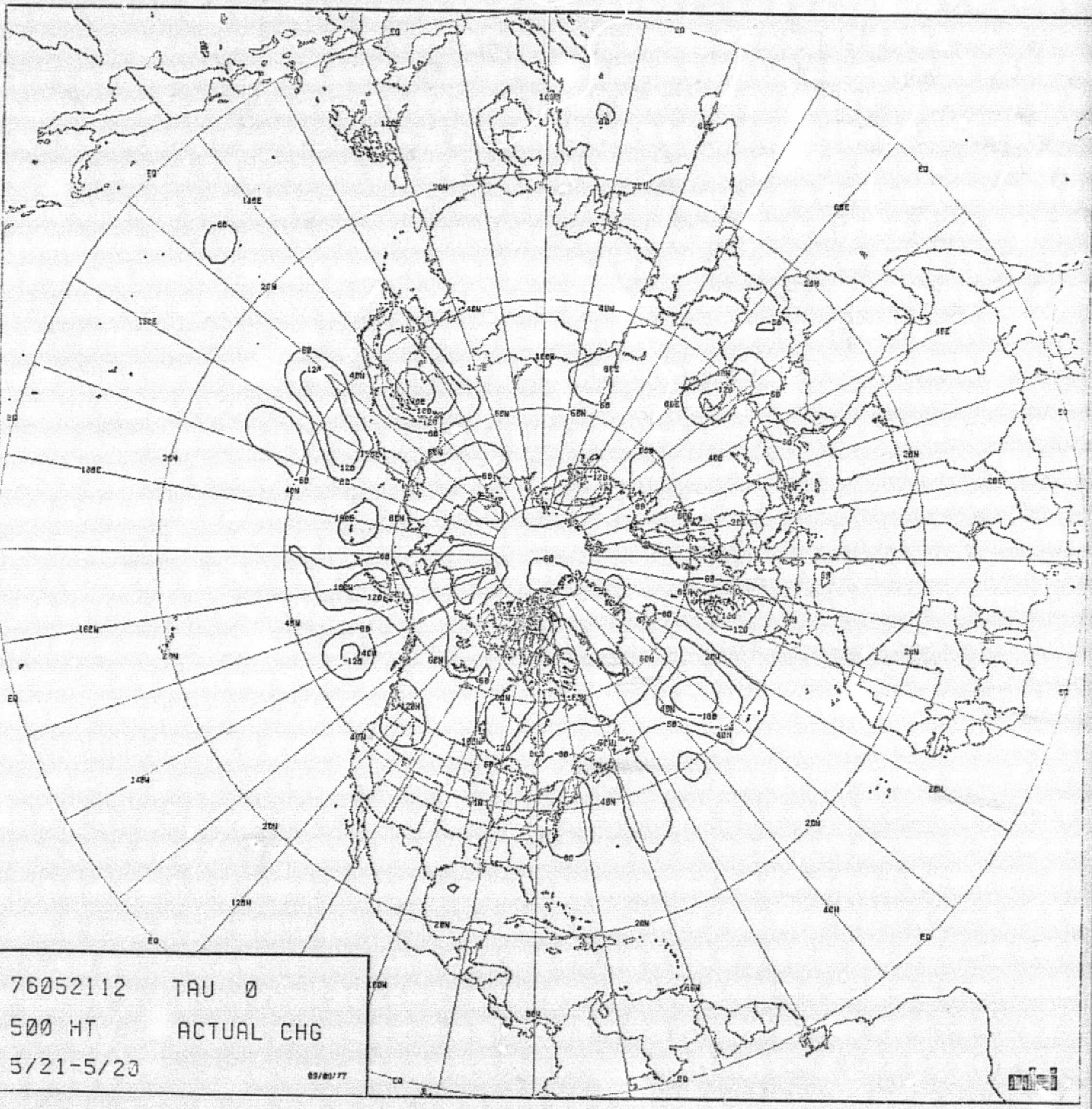

CHART VI-4: 500MB HEIGHT ACTUAL CHANGE, 1200Z, 5/21 - 5/20.

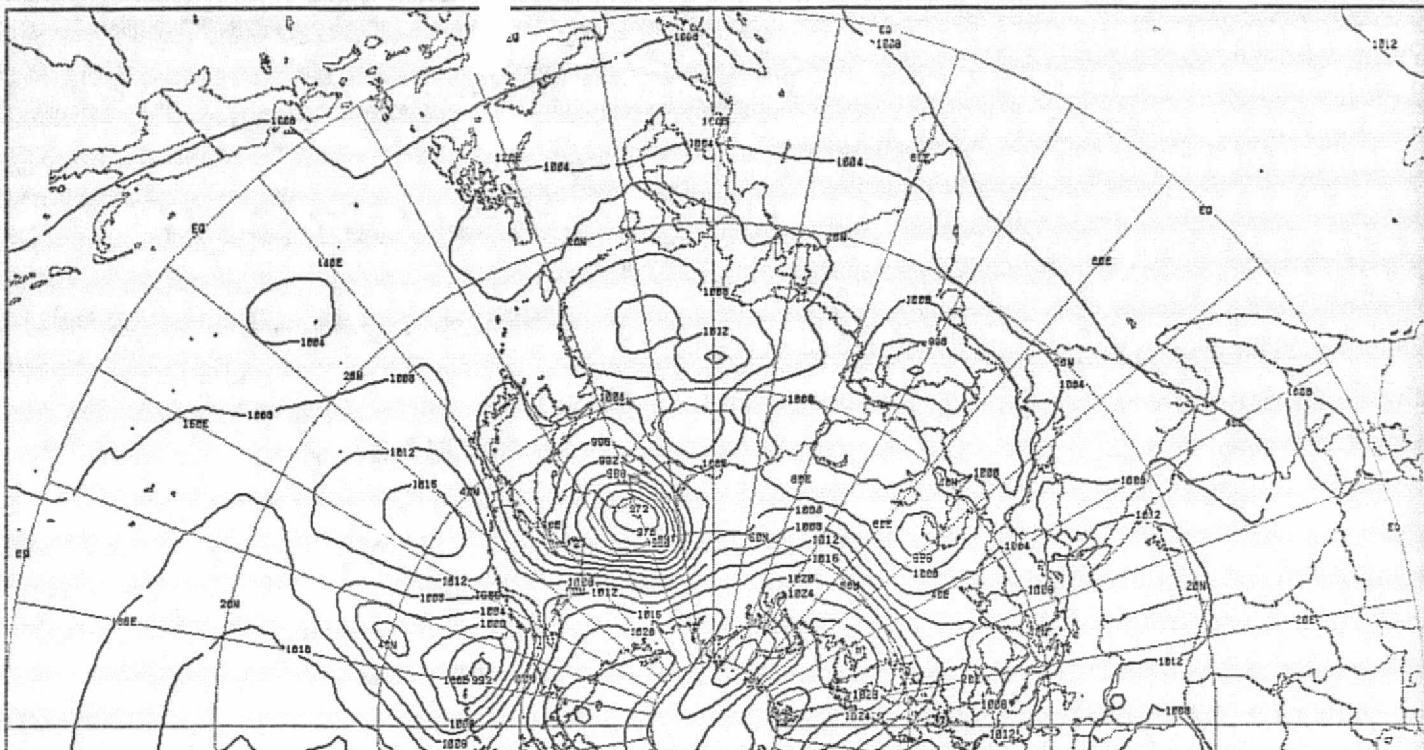

CHART VI-5: SEA-LEVEL PRESSURE 24-HOUR FORECAST, VERIF TIME 1200Z, 21 MAY 1976. RUN T9.

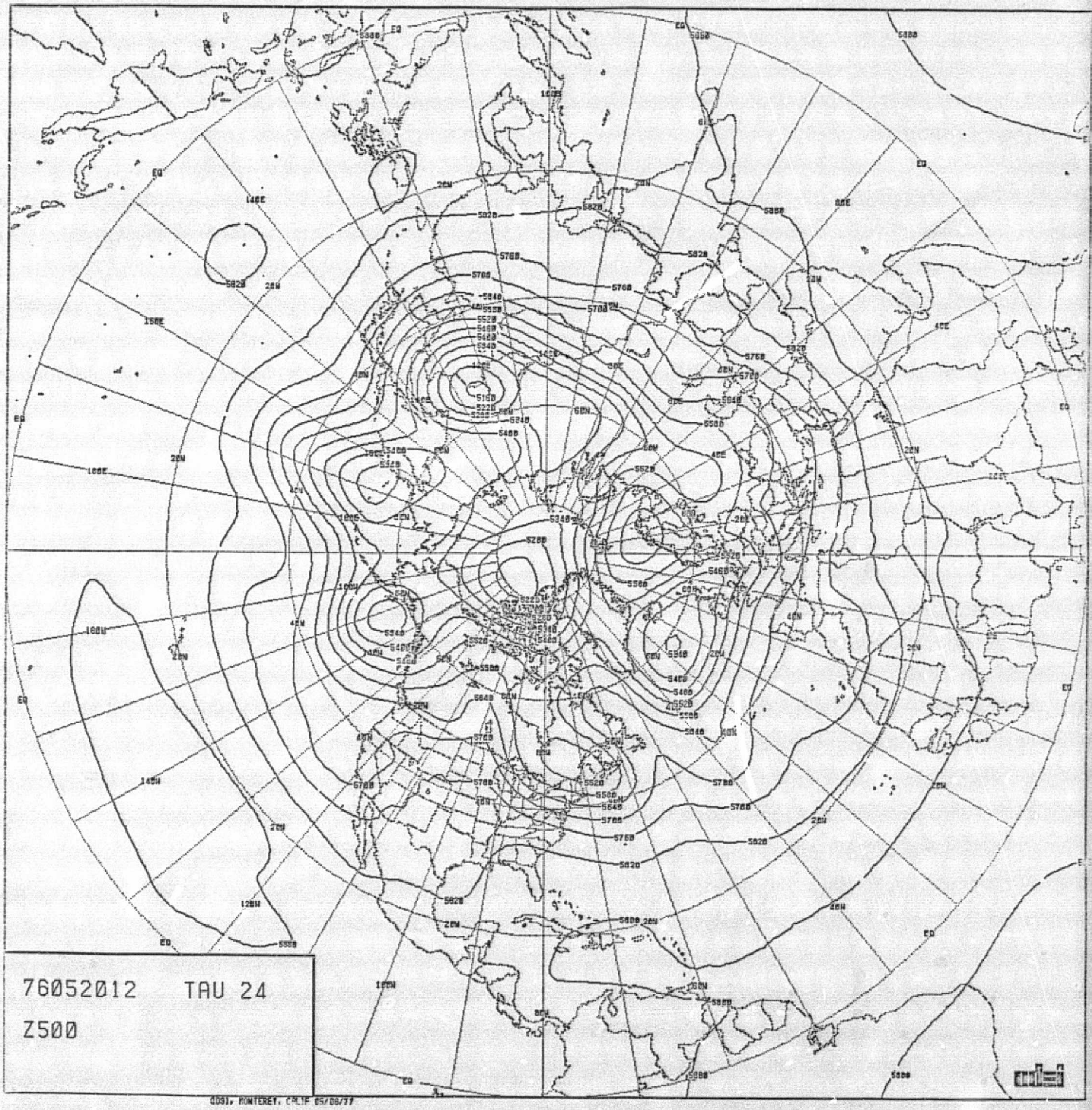

CHART VI-6: 500MB HEIGHT 24-HOUR FORECAST, VERIF TIME 1200Z, 21 MAY 1976. RUN T9.

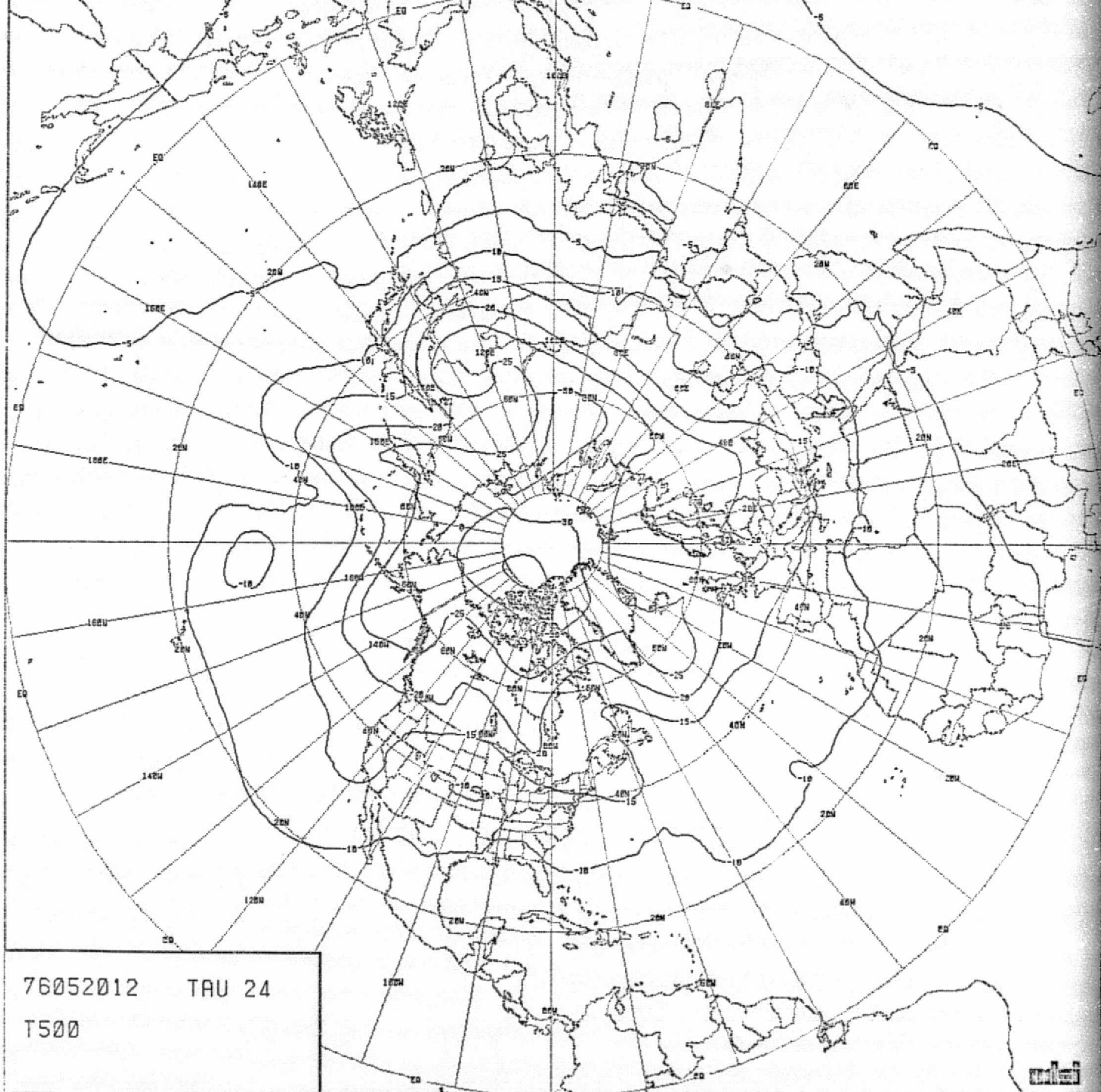

CHART VI-7: 500MB TEMPERATURE 24-HOUR FORECAST, VERIF TIME 1200Z, 21 MAY 1976. RUN T9.

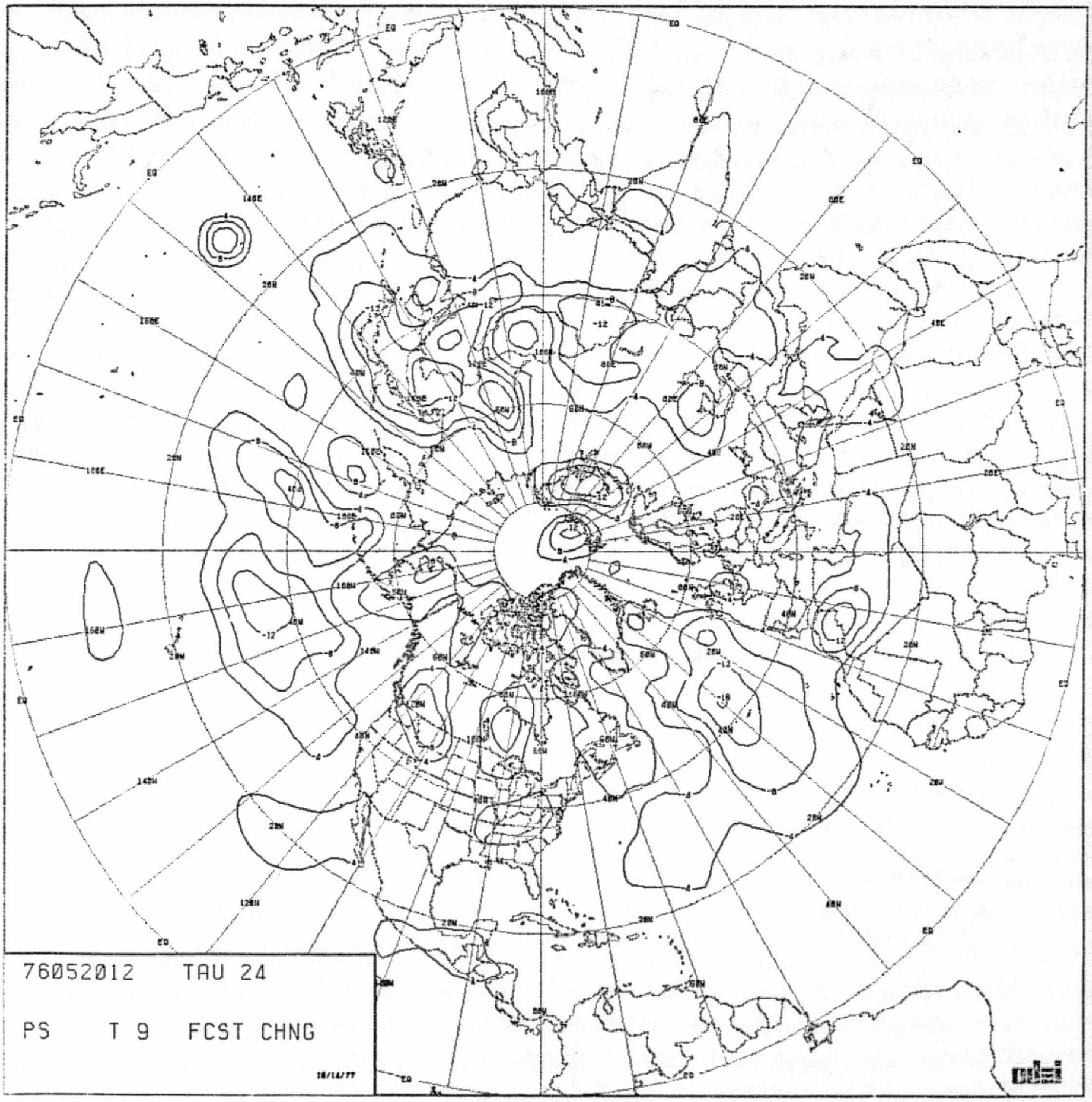

CHART VI-8: 24-HOUR FORECAST CHANGE. RUN T9. SEA-LEVEL PRESSURE.

ORIGINAL PAGE IS
OF POOR QUALITY

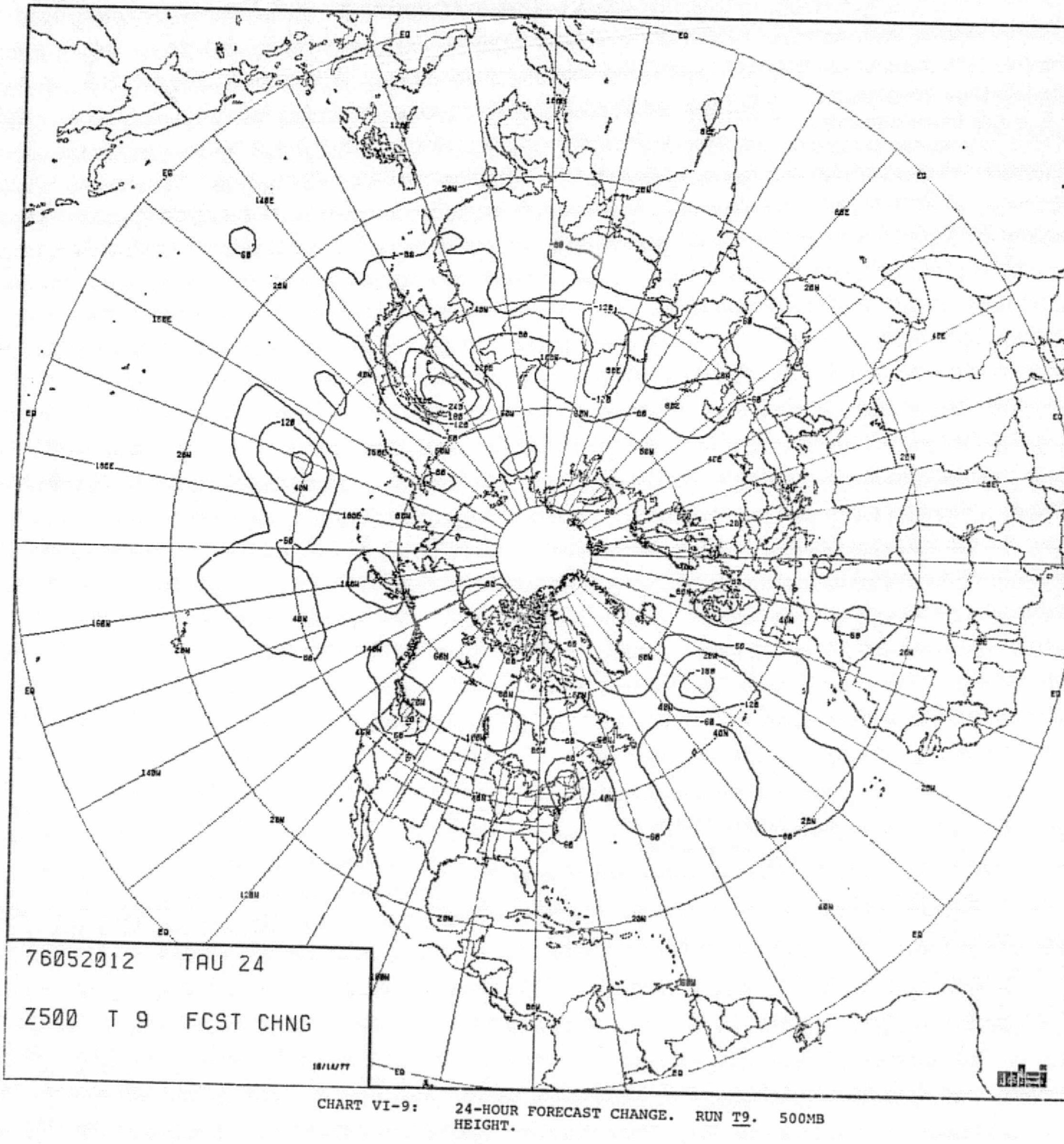

CHART VI-9: 24-HOUR FORECAST CHANGE. RUN T9. 500MB HEIGHT.

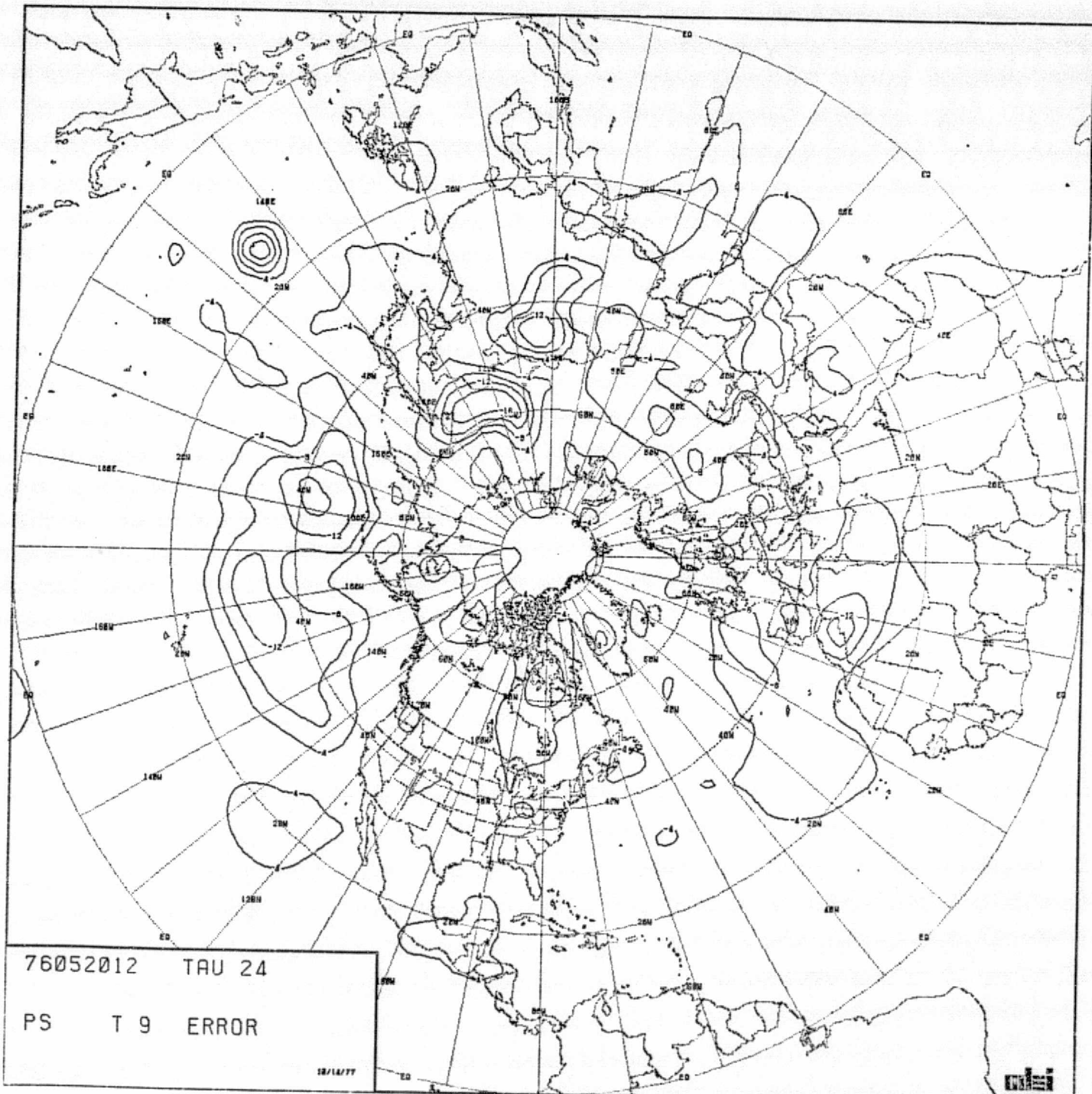

CHART VI-10: 24-HOUR FORECAST ERROR. RUN T9. SEA-LEVEL PRESSURE.

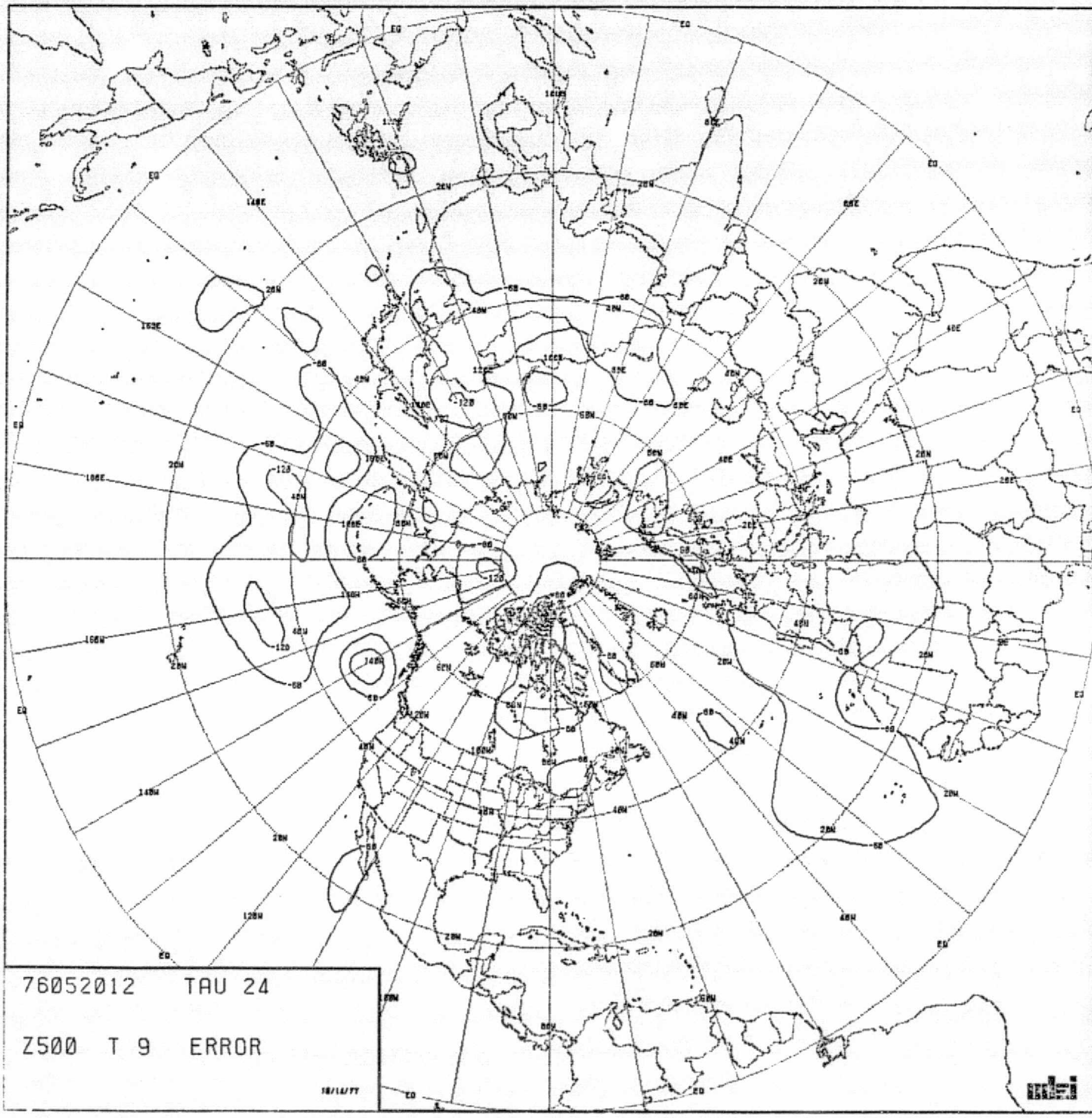

CHART VI-11: 24-HOUR FORECAST ERROR. RUN T9. 500MB HEIGHT.

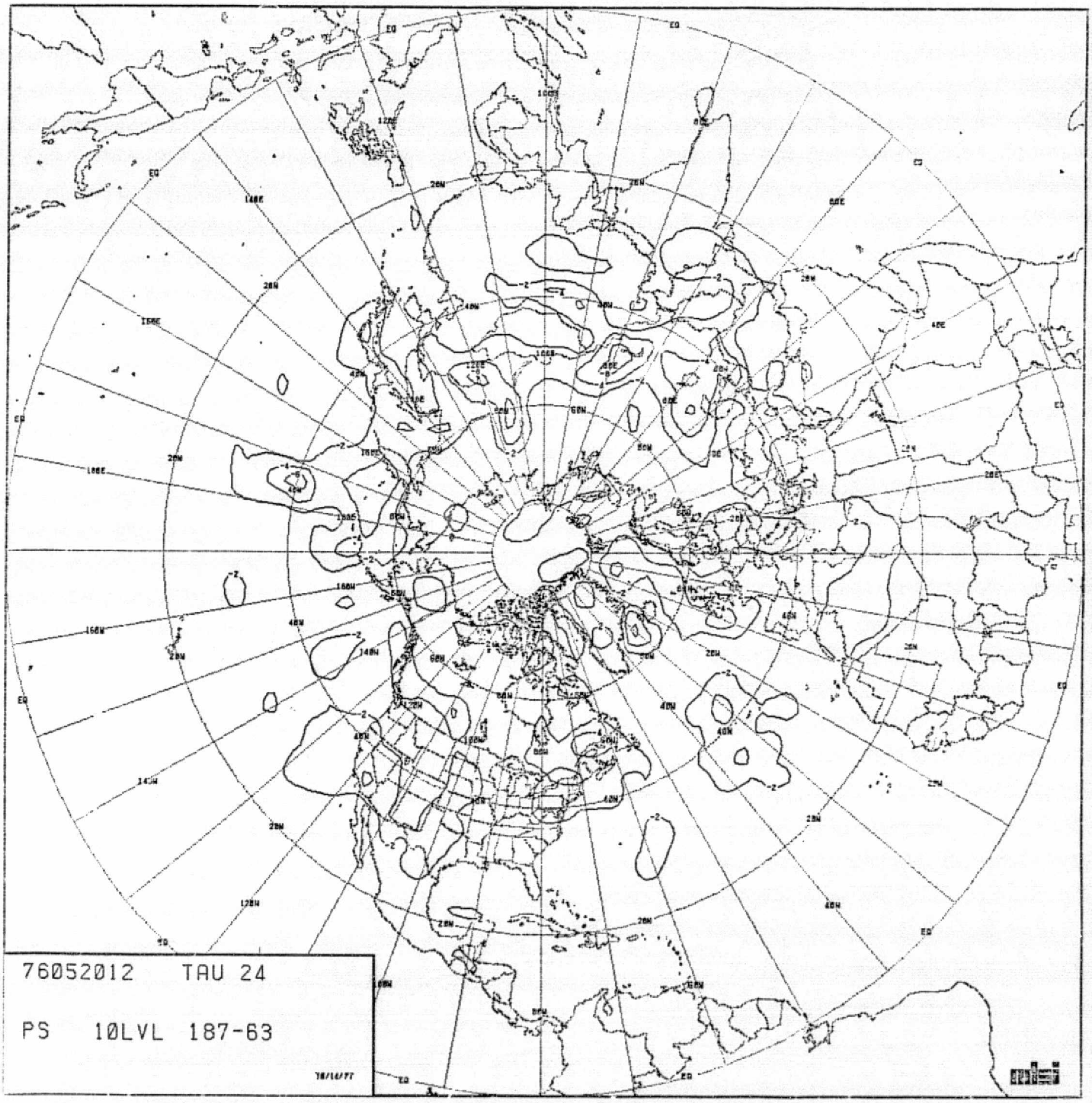

CHART VI-12: 24-HOUR SEA-LEVEL PRESSURE FMG (RUN T9) FORECAST MINUS CMG (RUN T5) FORECAST. SCENARIO B.

ORIGINAL PAGE IS
OF POOR QUALITY

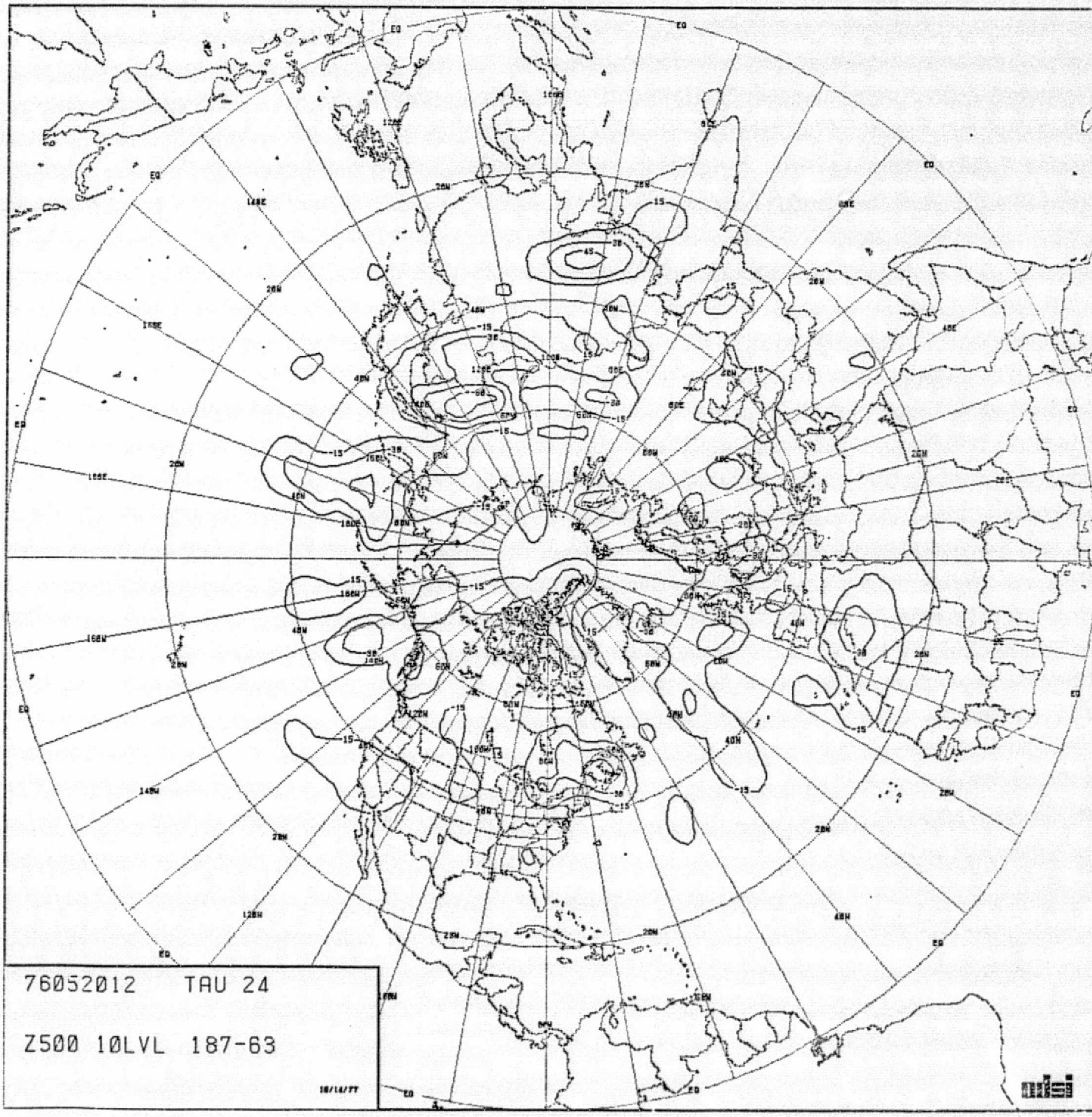

CHART VI-13: 24-HOUR 500MB HEIGHT (Z500) FMG (RUN T9) FORECA^T MINUS CMG (RUN T5) FORECAST. SCENAR.) B.

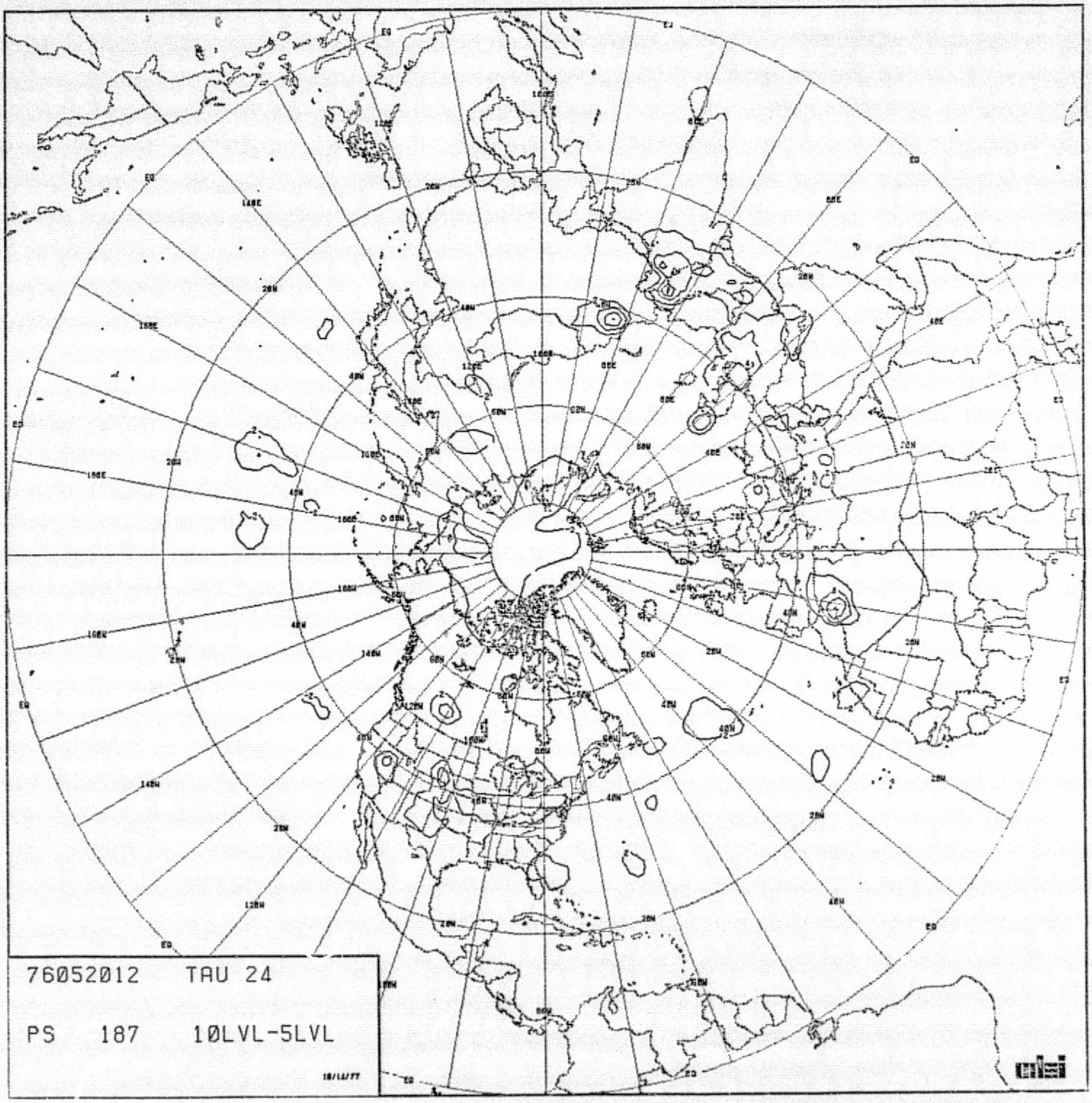

CHART VI-14: 24-HOUR FMG SEA-LEVEL PRESSURE TEN-LEVEL FORECAST (RUN T9) MINUS FIVE-LEVEL FORECAST (RUN F22). SCENARIO B.

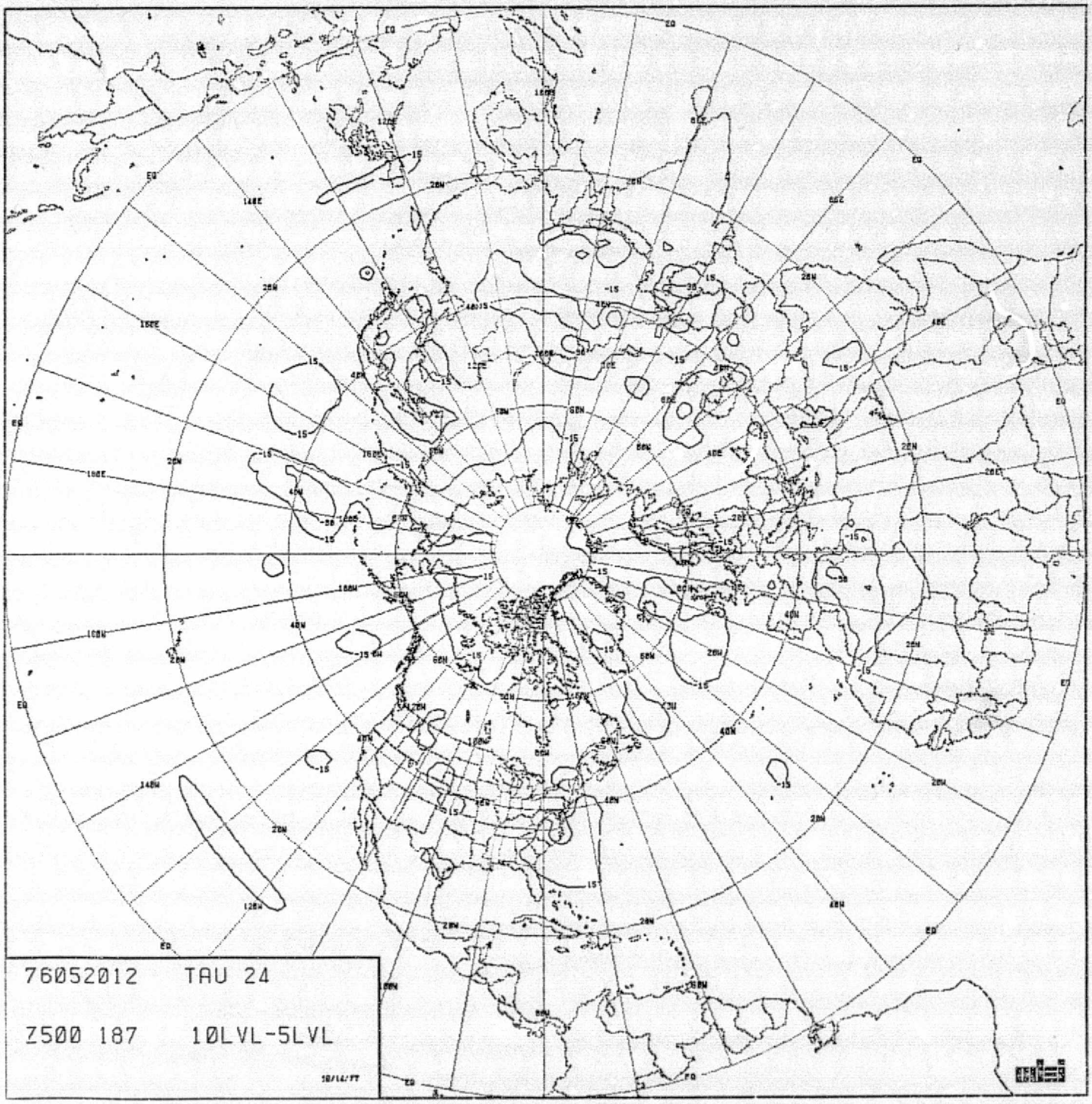

CHART VI-15: 24-HOUR FMG 500MB HEIGHT TEN-LEVEL FORECAST (RUN T9) MINUS FIVE-LEVEL FORECAST (RUN F22). SCENARIO B.

VII. FIGURES

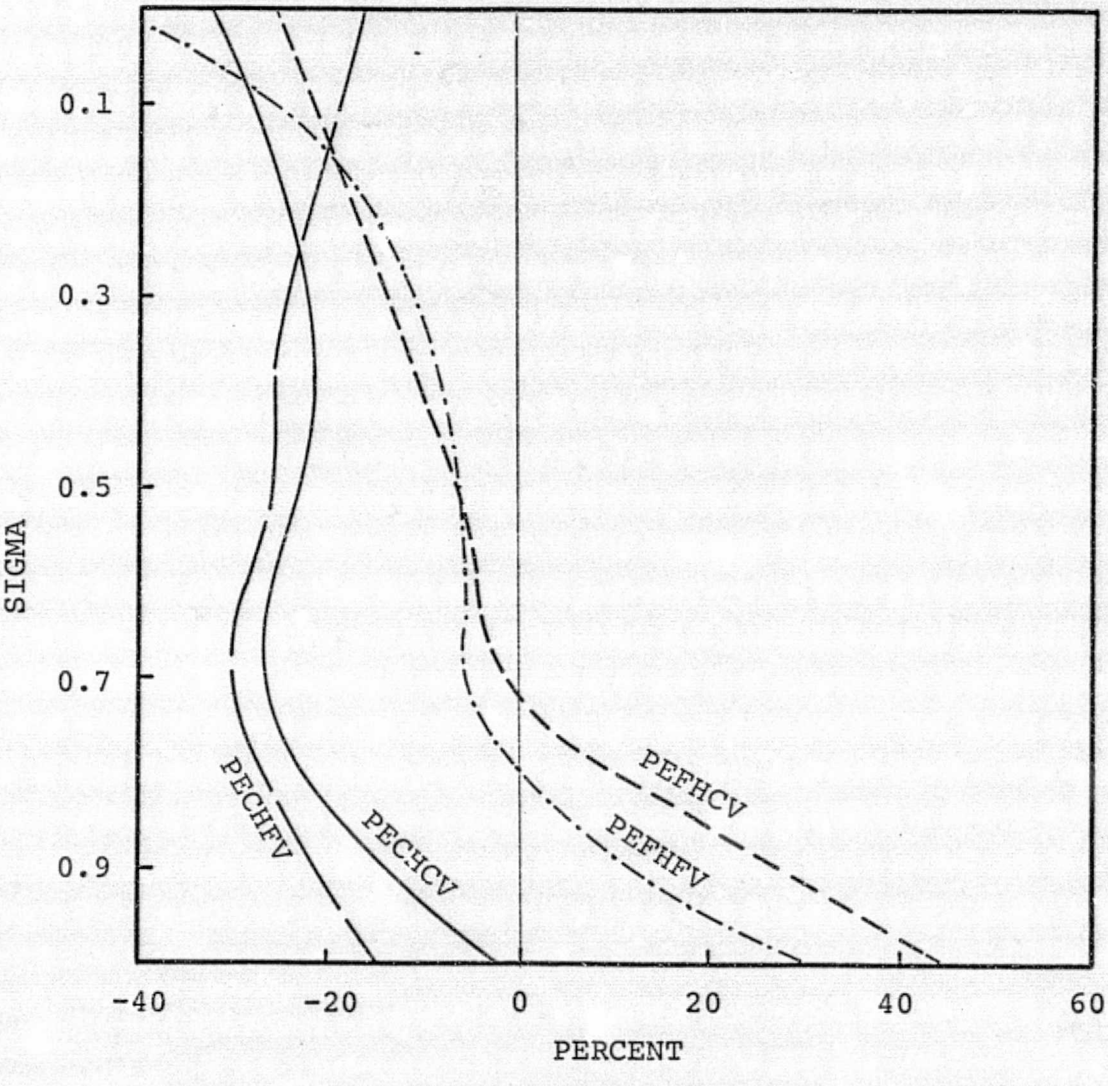

FIGURE VII-1: KINETIC ENERGY 24-HOUR FORECAST CHANGE (%), BY MODEL VERSION AND LEVEL. SCENARIO B.

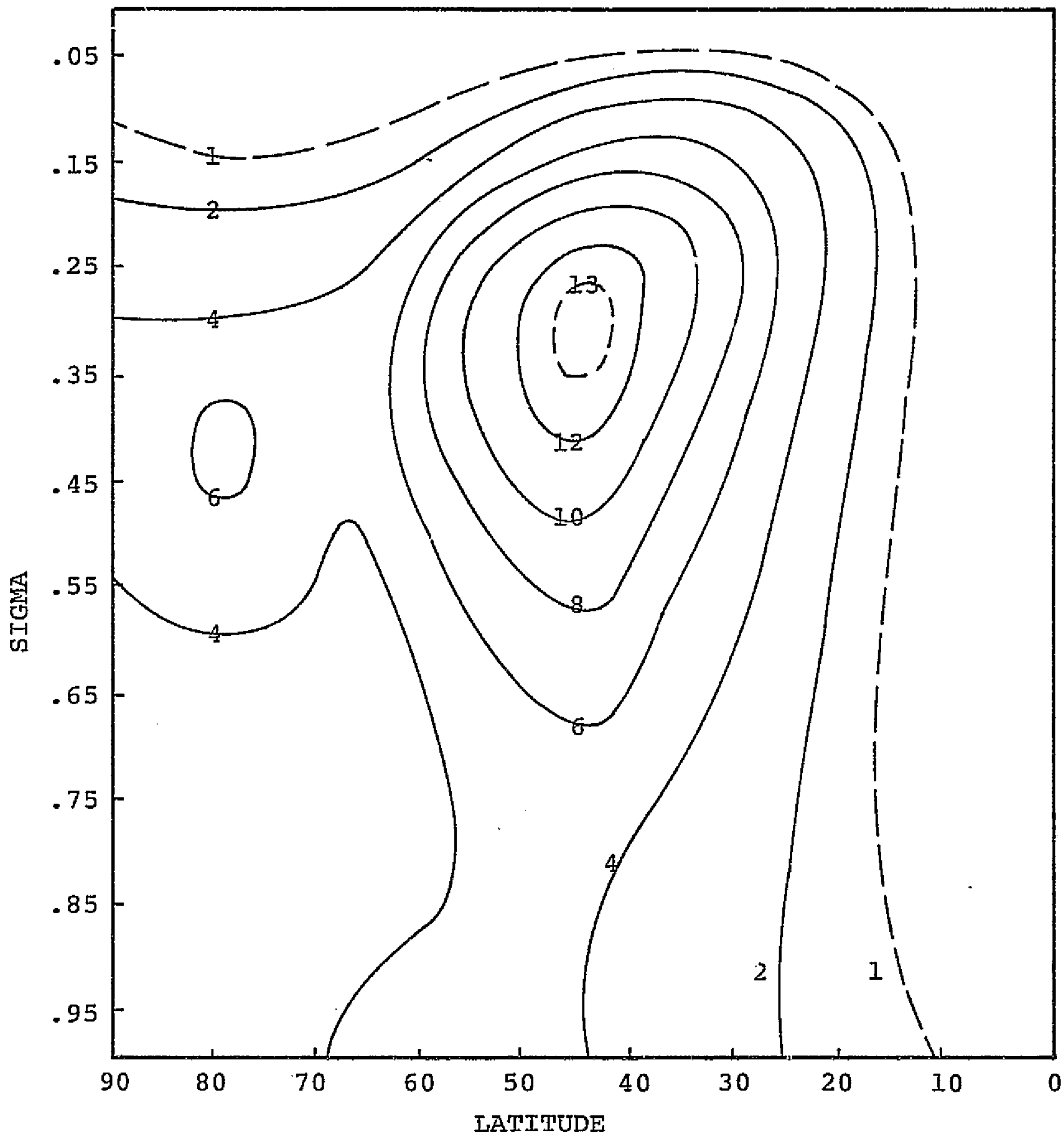

FIGURE VII-2: KINETIC ENERGY (x10) 24-HOUR FORECAST CROSS-SECTION. RUN T9. MODEL PEFHFV. SCENARIO B.

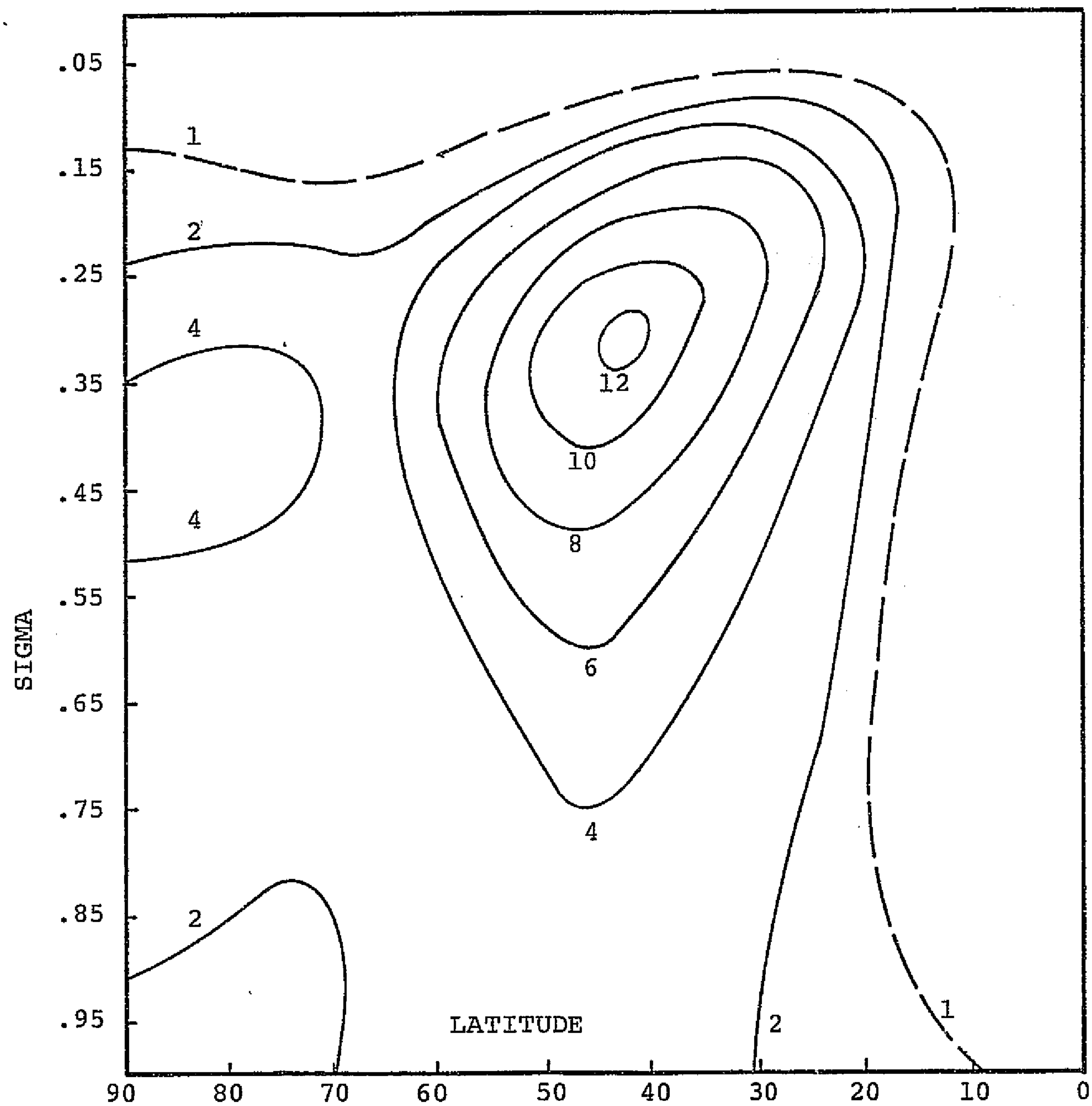

FIGURE VII-3: KINETIC ENERGY (x10) 24-HOUR FORECAST CROSS-SECTION. RUN T5. MODEL PECHFV. SCENARIO B.

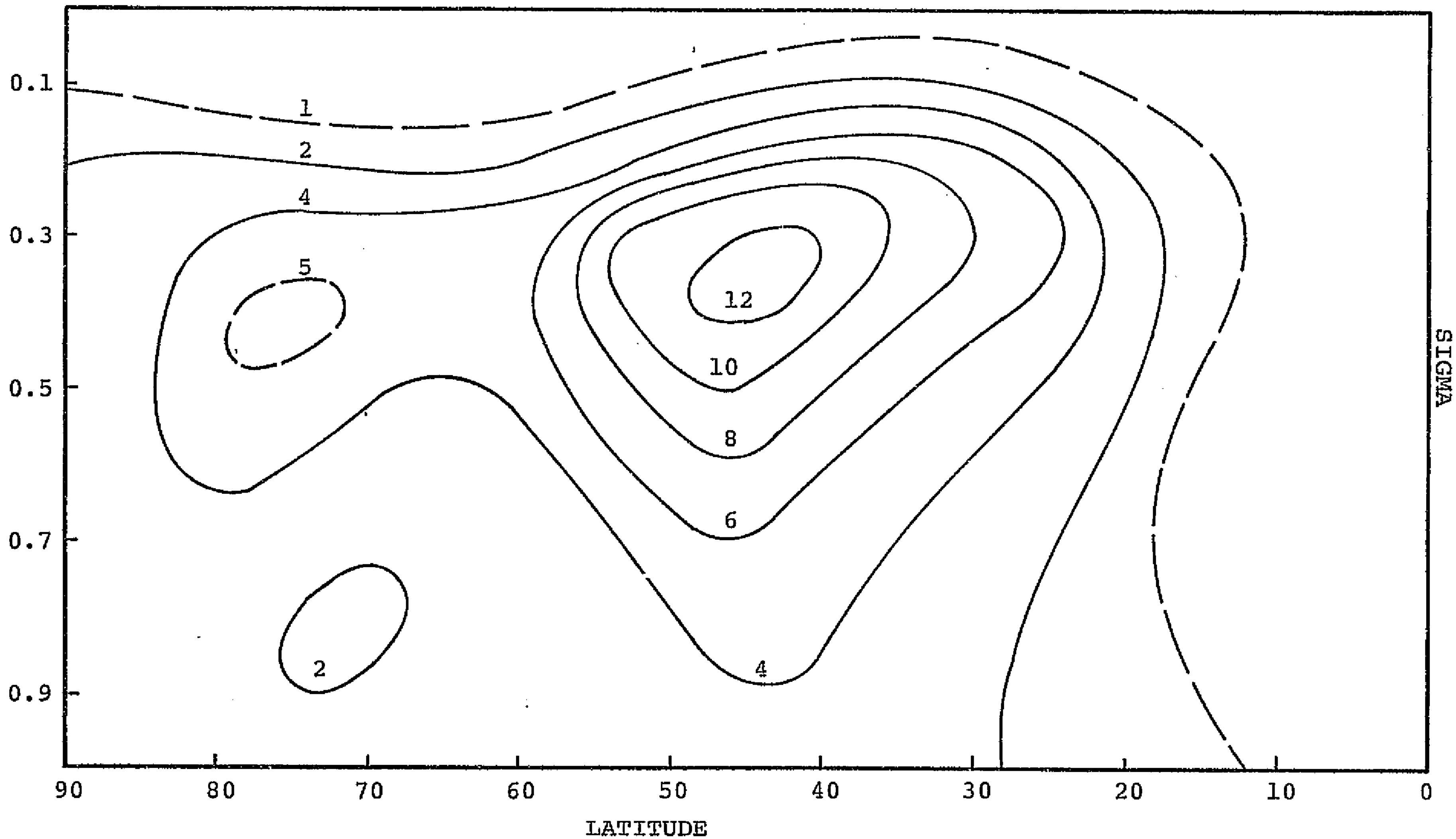

FIGURE VII-4: KINETIC ENERGY (x10) 24-HOUR FORECAST CROSS-SECTION. RUN F19. MODEL PECHCV. SCENARIO B.

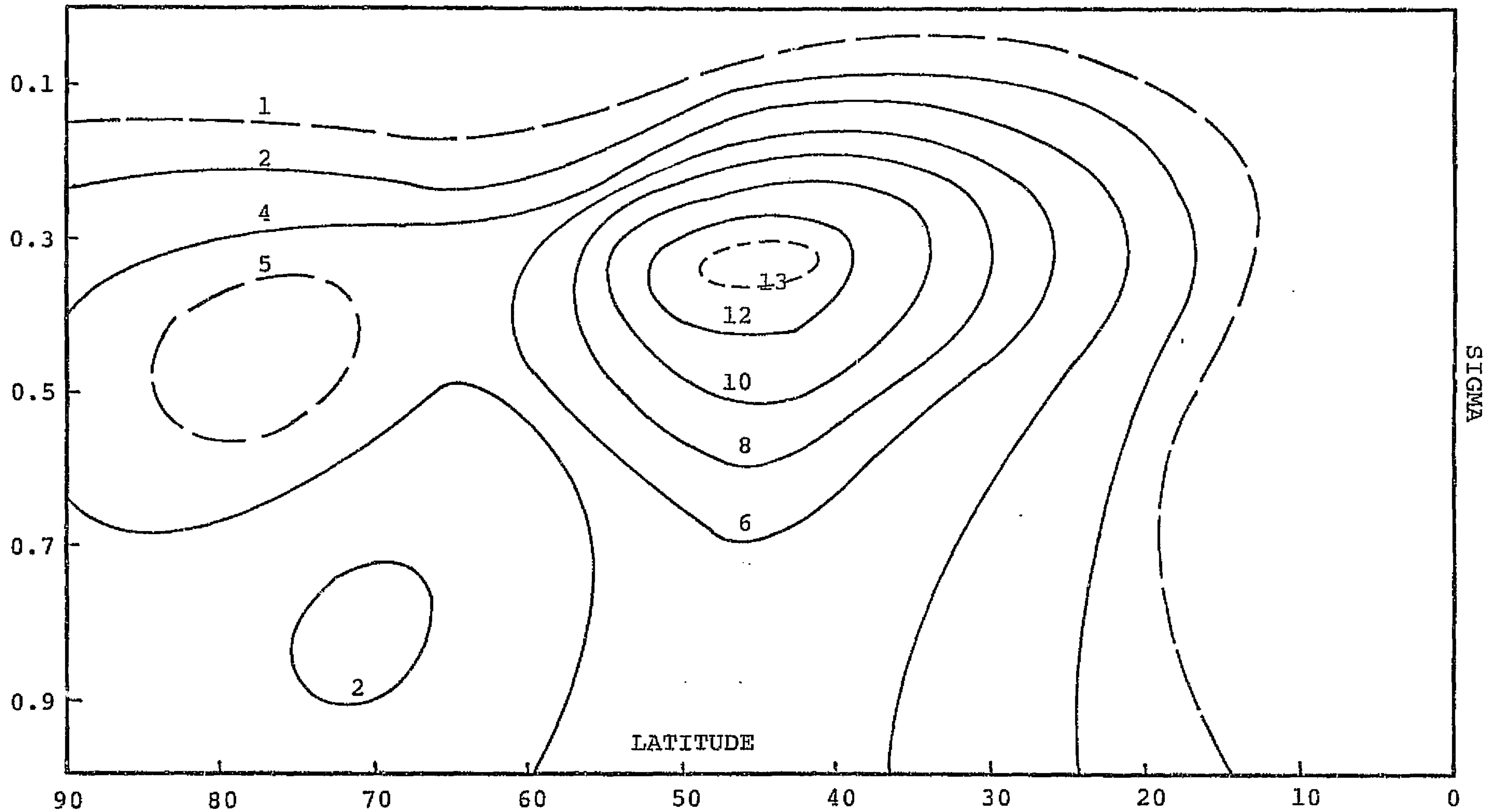

FIGURE VII-5: KINETIC ENERGY (x10) 24-HOUR FORECAST CROSS-SECTION. RUN F24. MODEL PEFHCV. SCENARIO B.

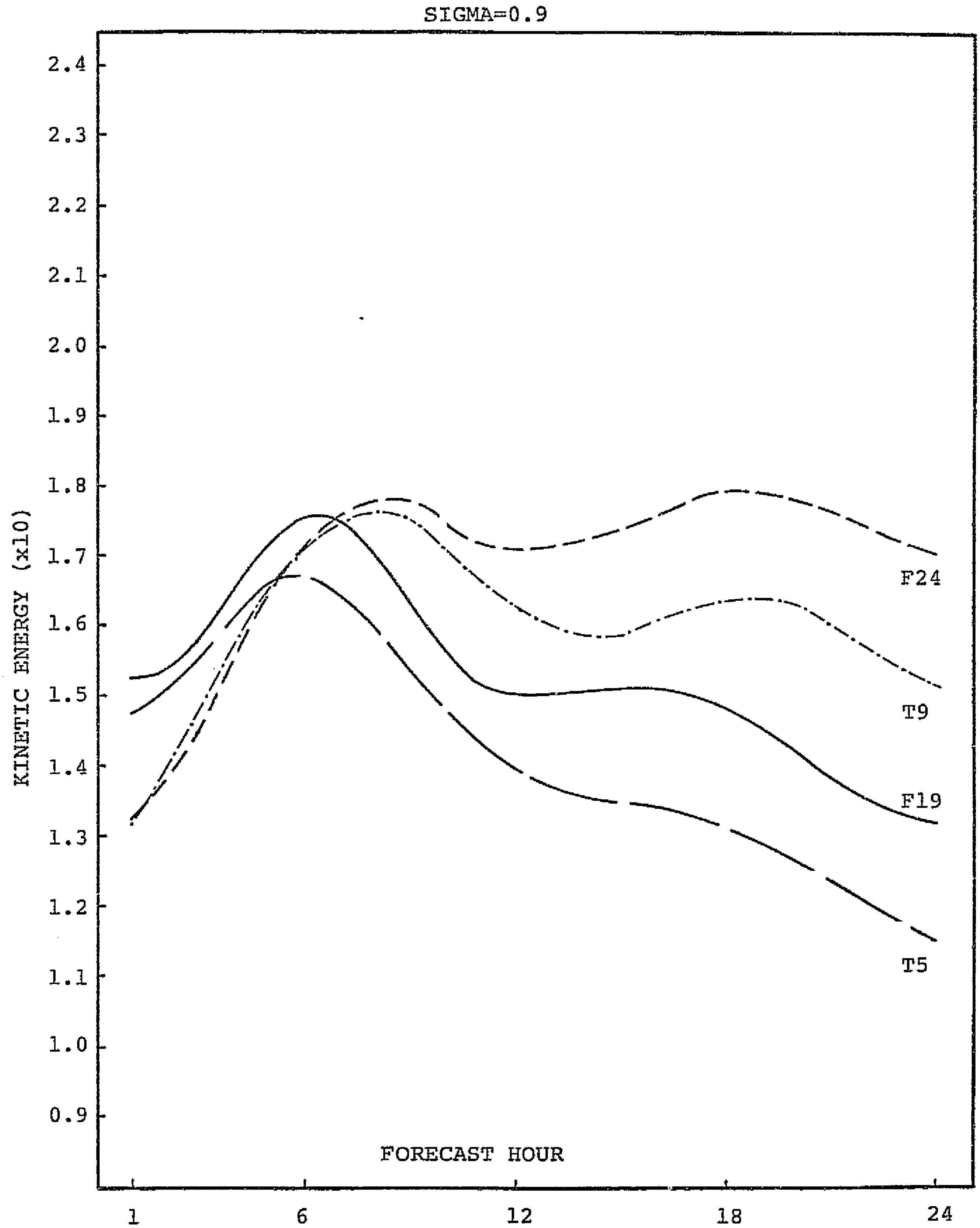

FIGURE VII-6: TIME VARIATION OF KINETIC ENERGY FOR FOUR MODEL VERSIONS AT SIGMA=0.9 LEVEL. SCENARIO B.

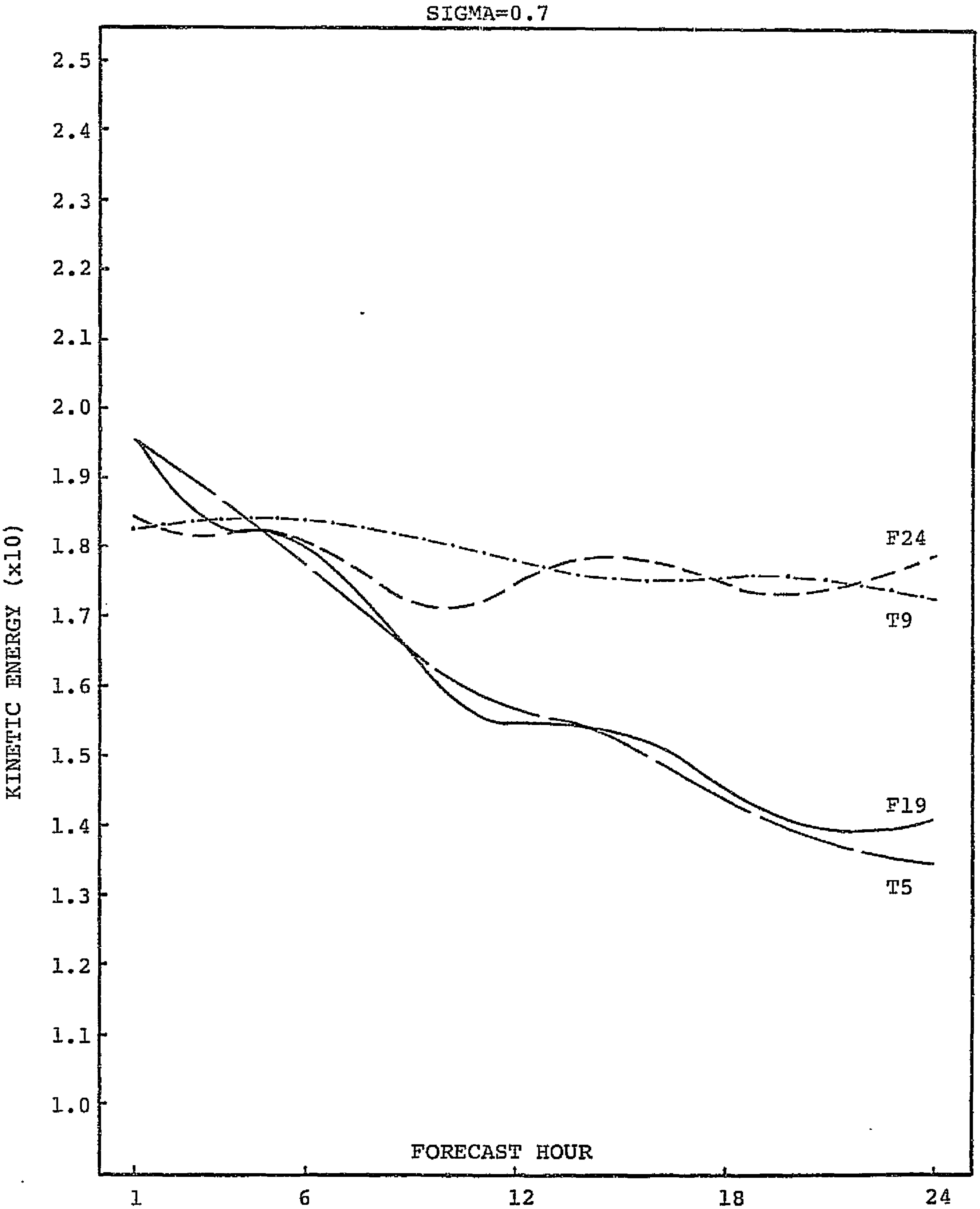

FIGURE VII-7: TIME VARIATION OF KINETIC ENERGY FOR FOUR MODEL VERSIONS AT SIGMA=0.7 LEVEL. SCENARIO B.

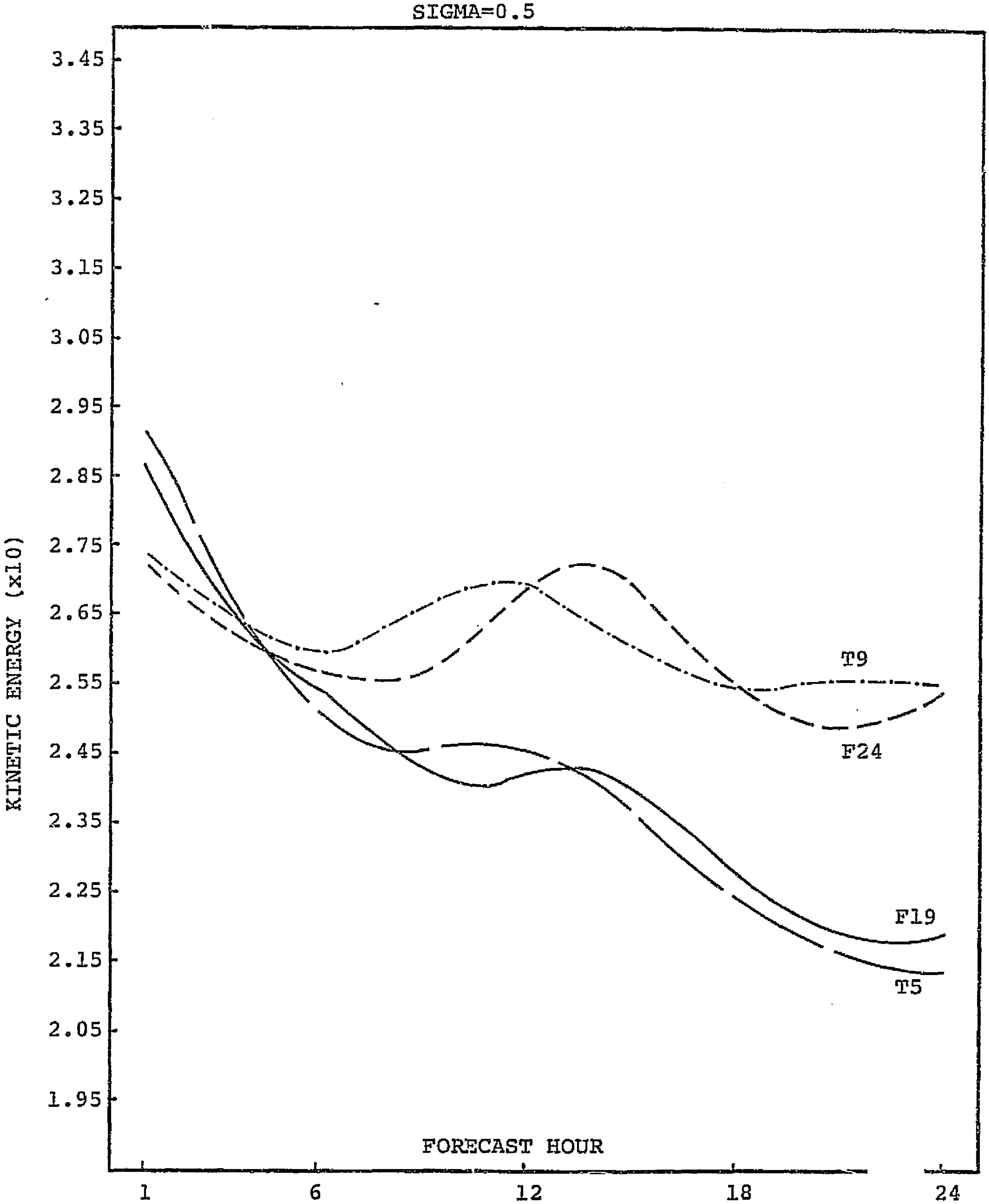

FIGURE VII-8: TIME VARIATION OF KINETIC ENERGY FOR FOUR MODEL VERSIONS AT SIGMA=0.5 LEVEL. SCENARIO B.

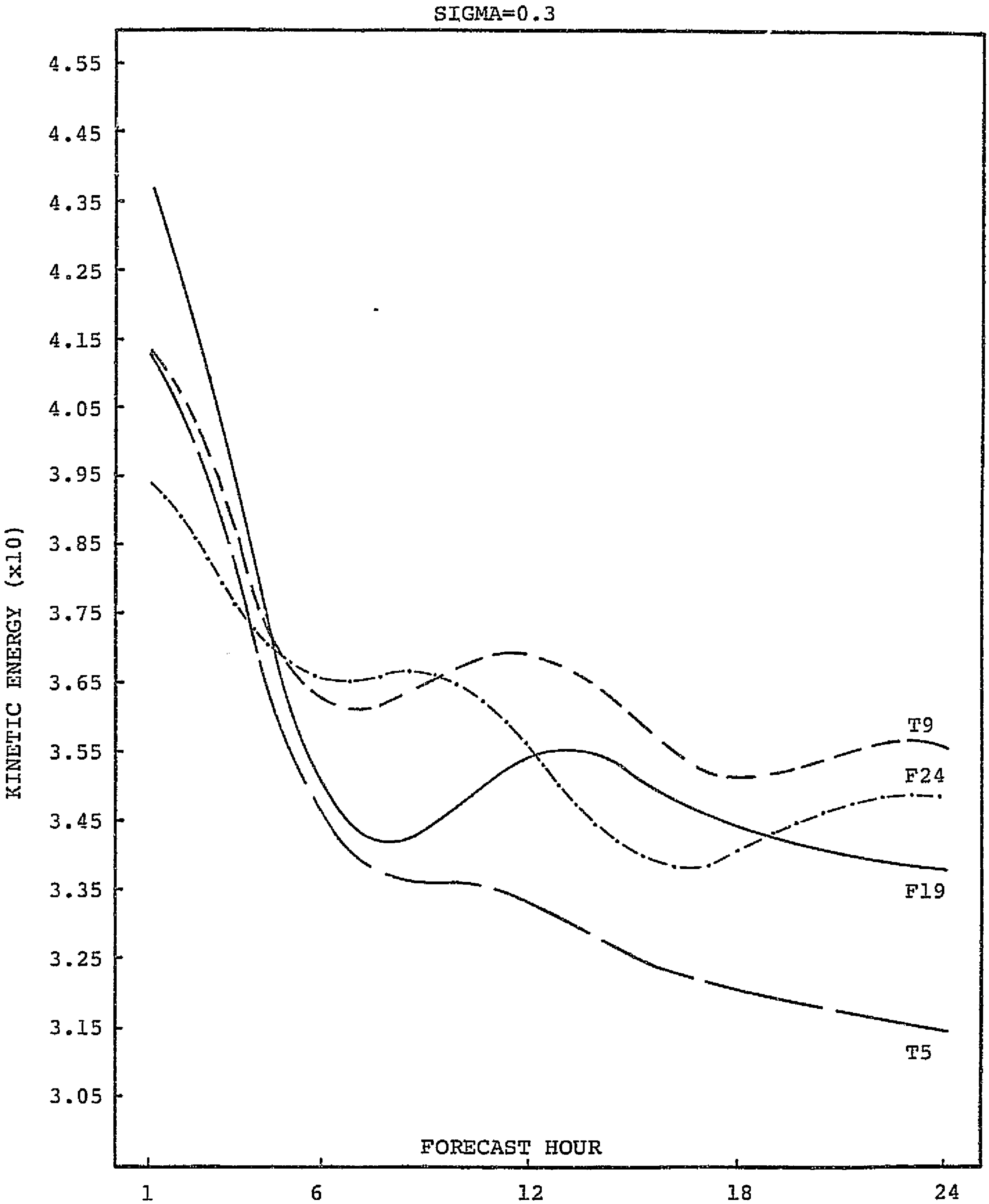

FIGURE VII-9: TIME VARIATION OF KINETIC ENERGY FOR FOUR MODEL VERSIONS AT SIGMA=0.3 LEVEL. SCENARIO <u>B</u>.

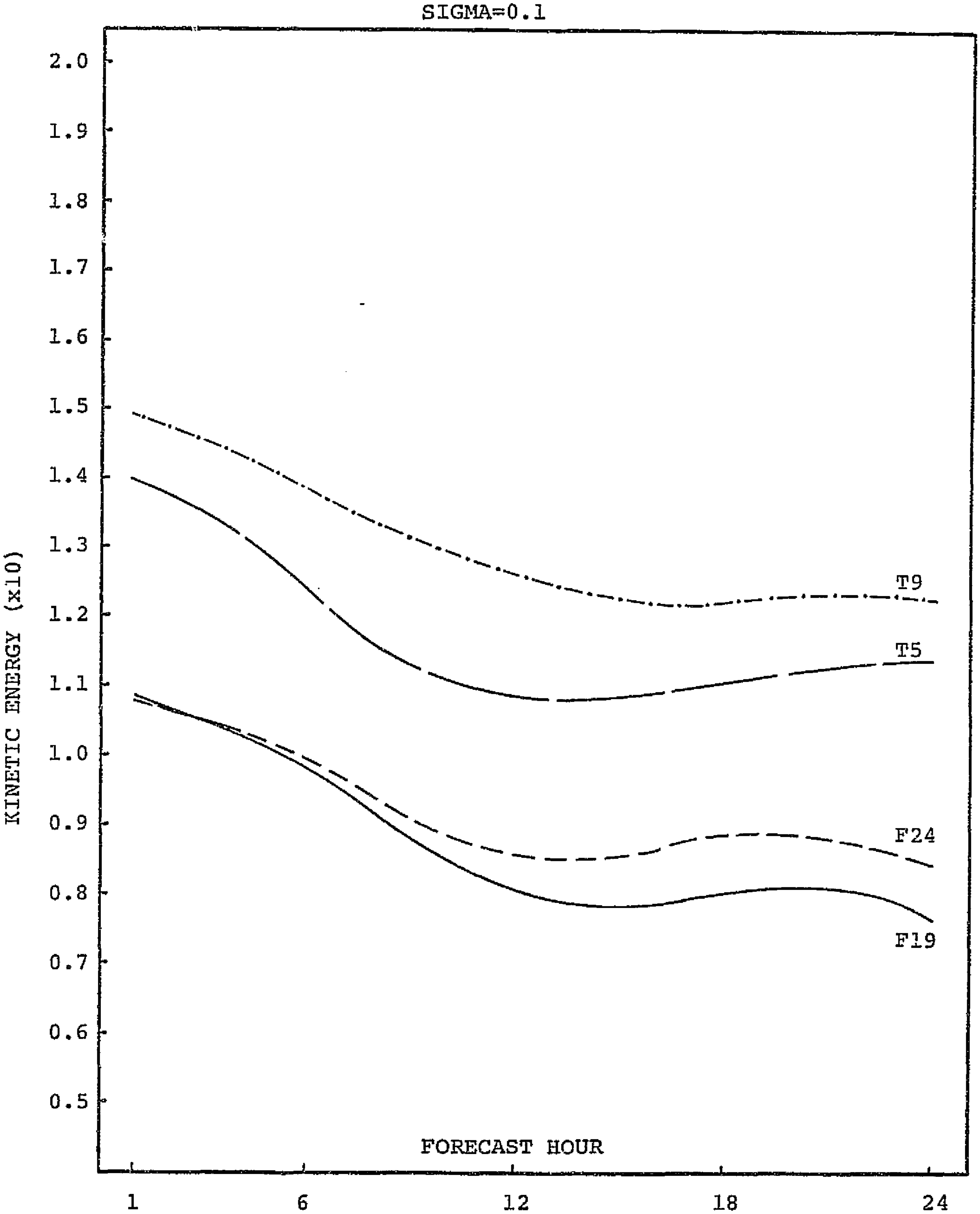

FIGURE VII-10: TIME VARIATION OF KINETIC ENERGY FOR FOUR MODEL VERSIONS AT SIGMA=0.1 LEVEL. SCENARIO B.

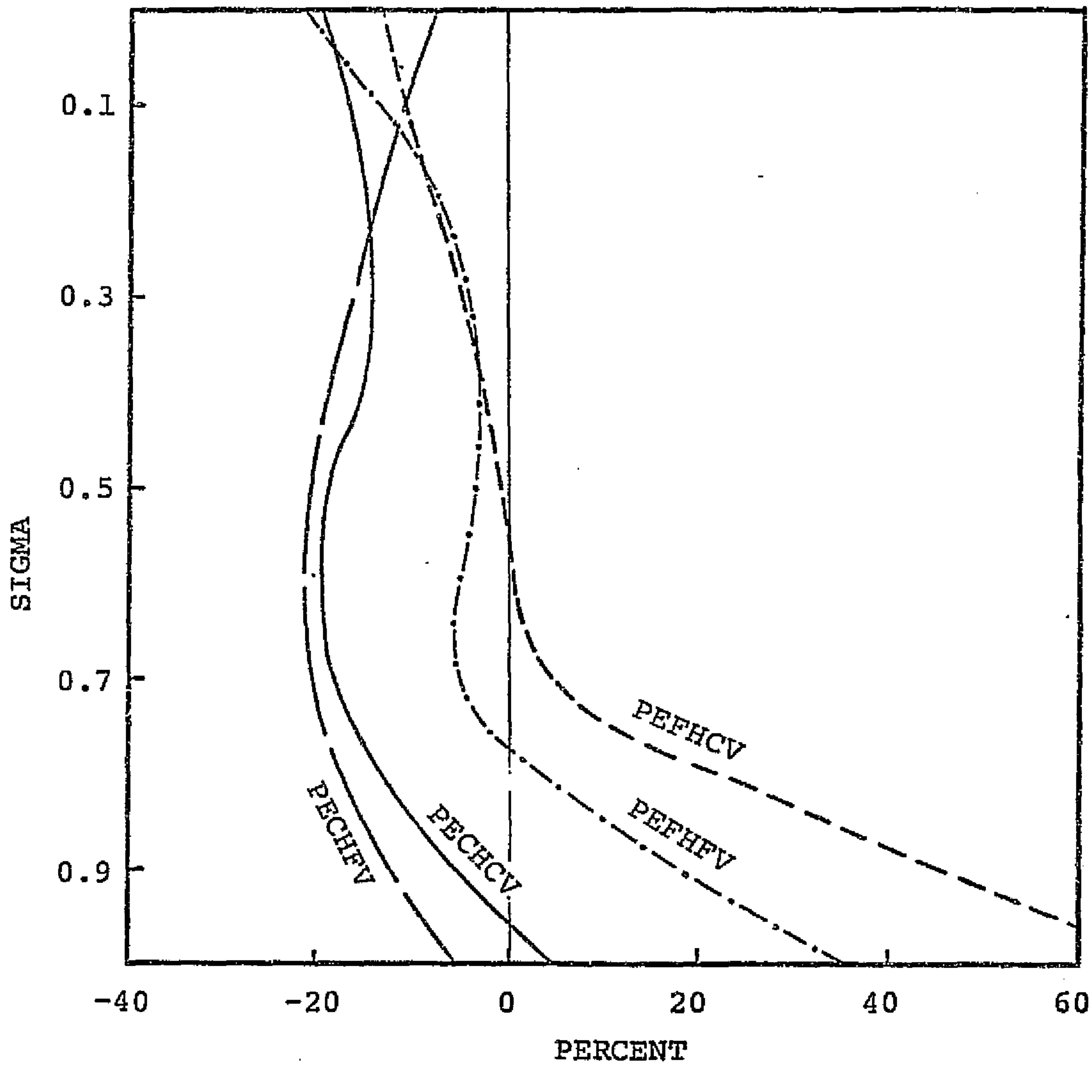

FIGURE VII-11: SQUARE VORTICITY 24-HOUR FORECAST CHANGE (%), BY MODEL VERSION AND LEVEL. SCENARIO B.

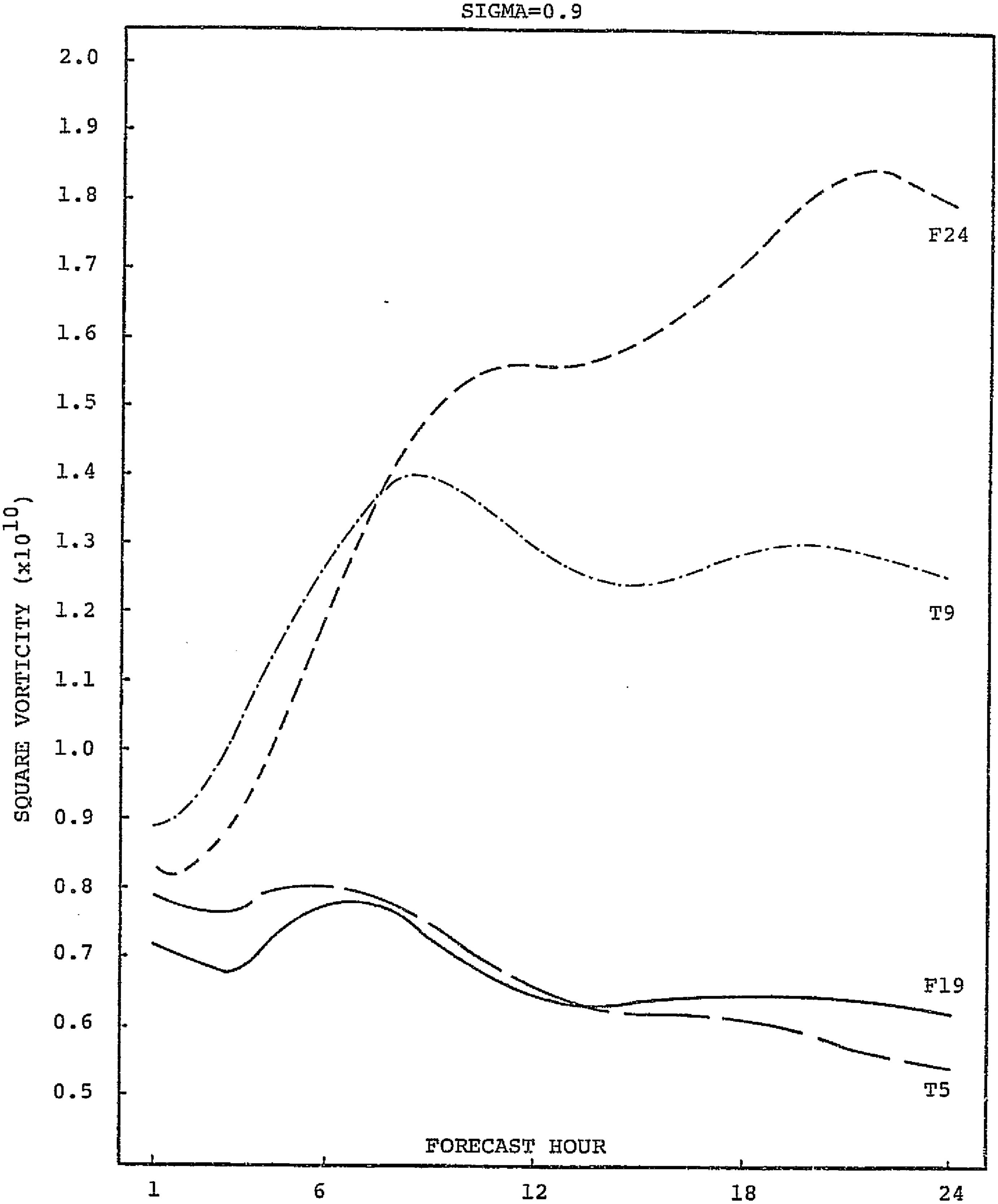

FIGURE VII-12: TIME VARIATION OF SQUARE VORTICITY FOR FOUR MODEL VERSIONS AT SIGMA=0.9 LEVEL. SCENARIO B.

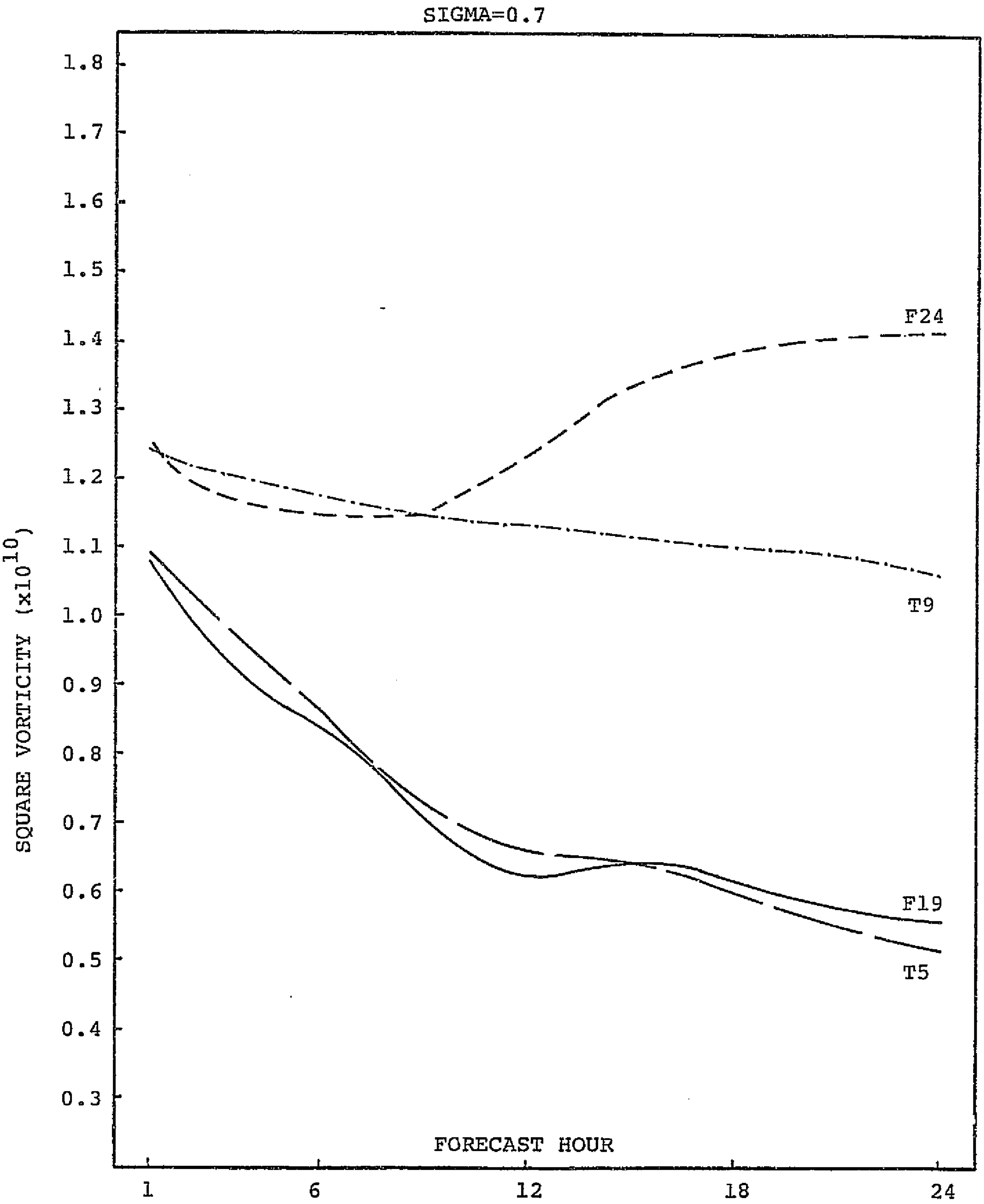

FIGURE VII-13: TIME VARIATION OF SQUARE VORTICITY FOR FOUR MODEL VERSIONS AT SIGMA=0.7 LEVEL. SCENARIO B.

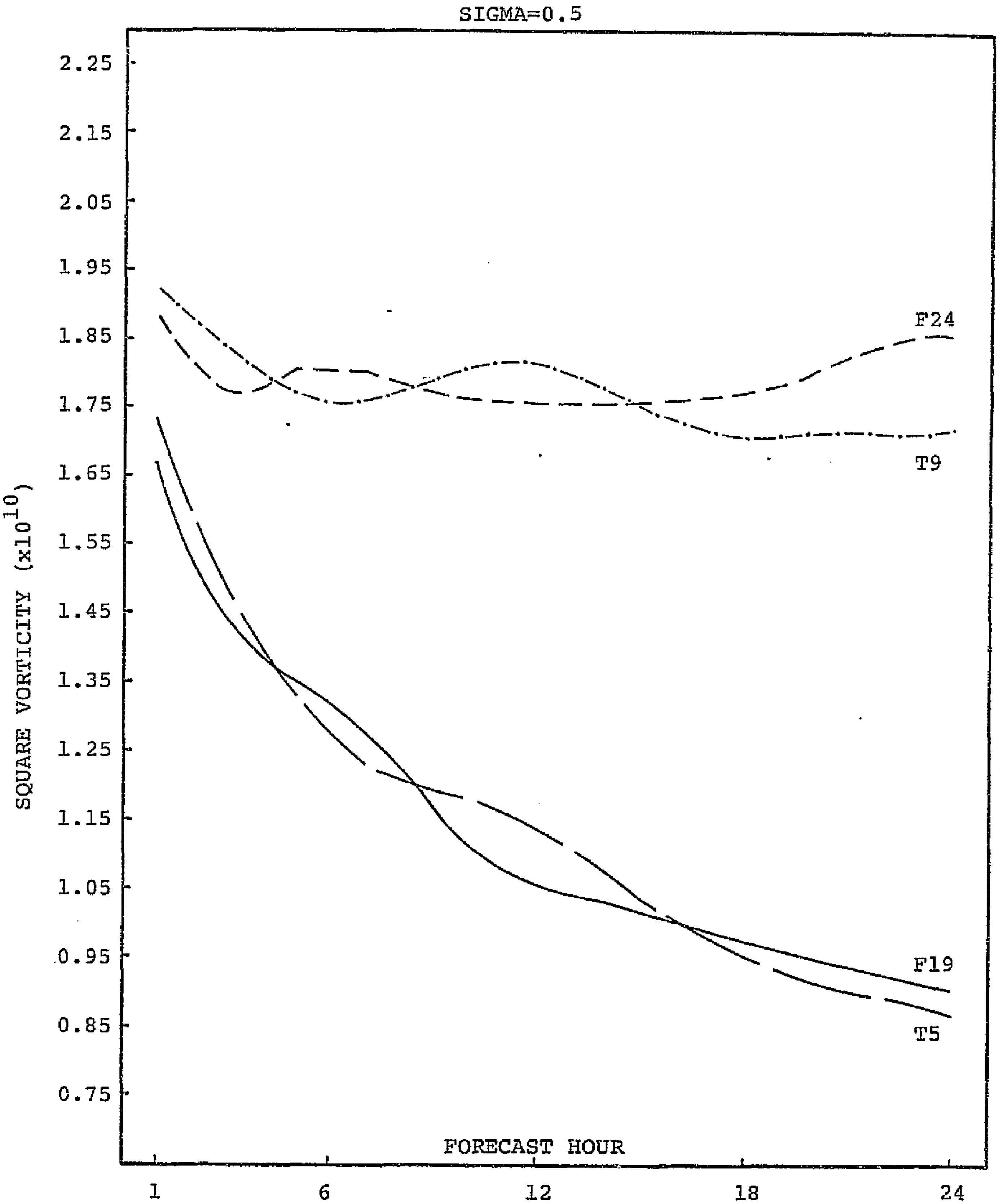

FIGURE VII-14: TIME VARIATION OF SQUARE VORTICITY FOR FOUR MODEL VERSIONS AT SIGMA=0.5 LEVEL. SCENARIO B.

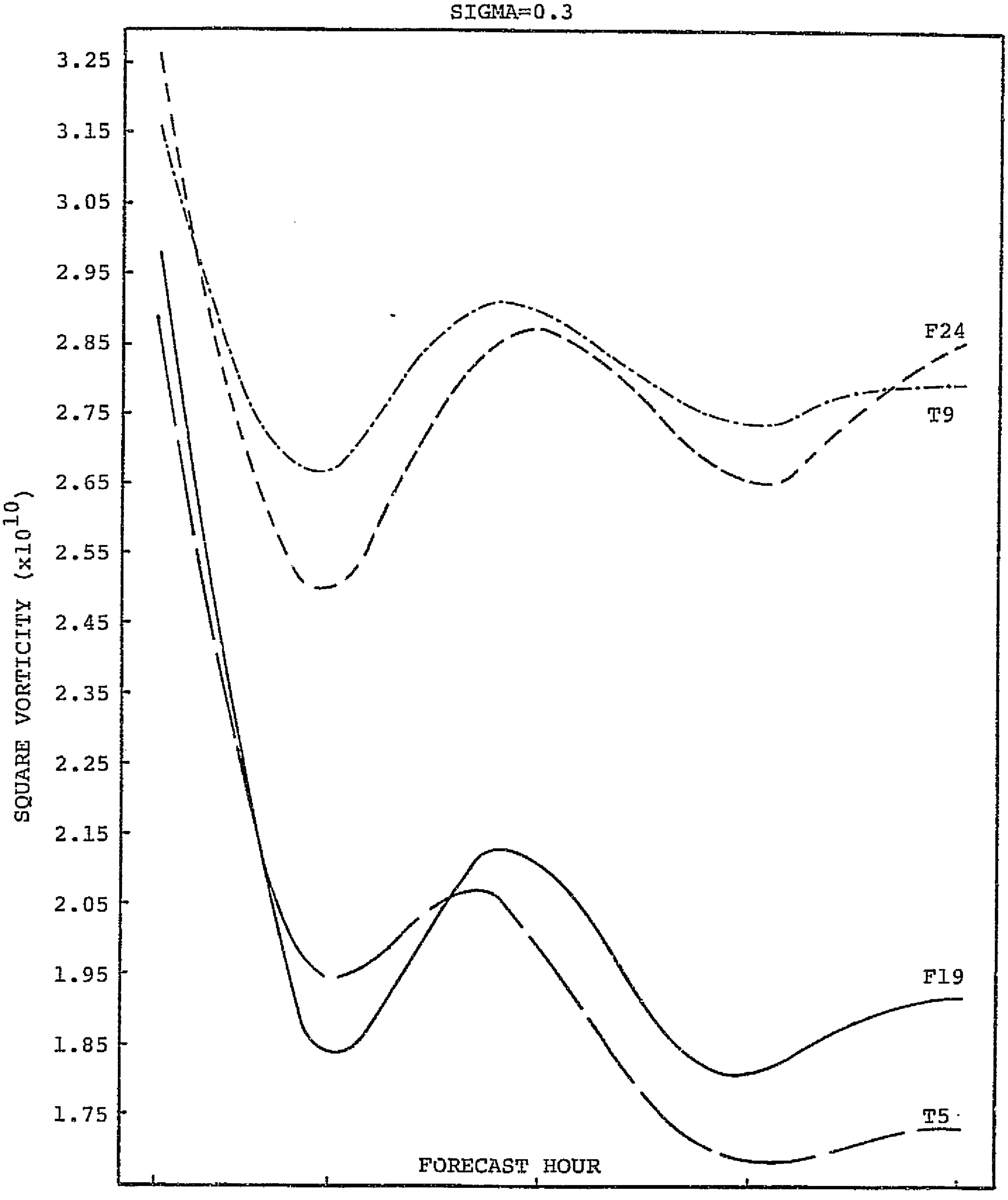

FIGURE VII-15: TIME VARIATION OF SQUARE VORTICITY FOR FOUR MODEL VERSIONS AT SIGMA=0.3 LEVEL. SCENARIO B.

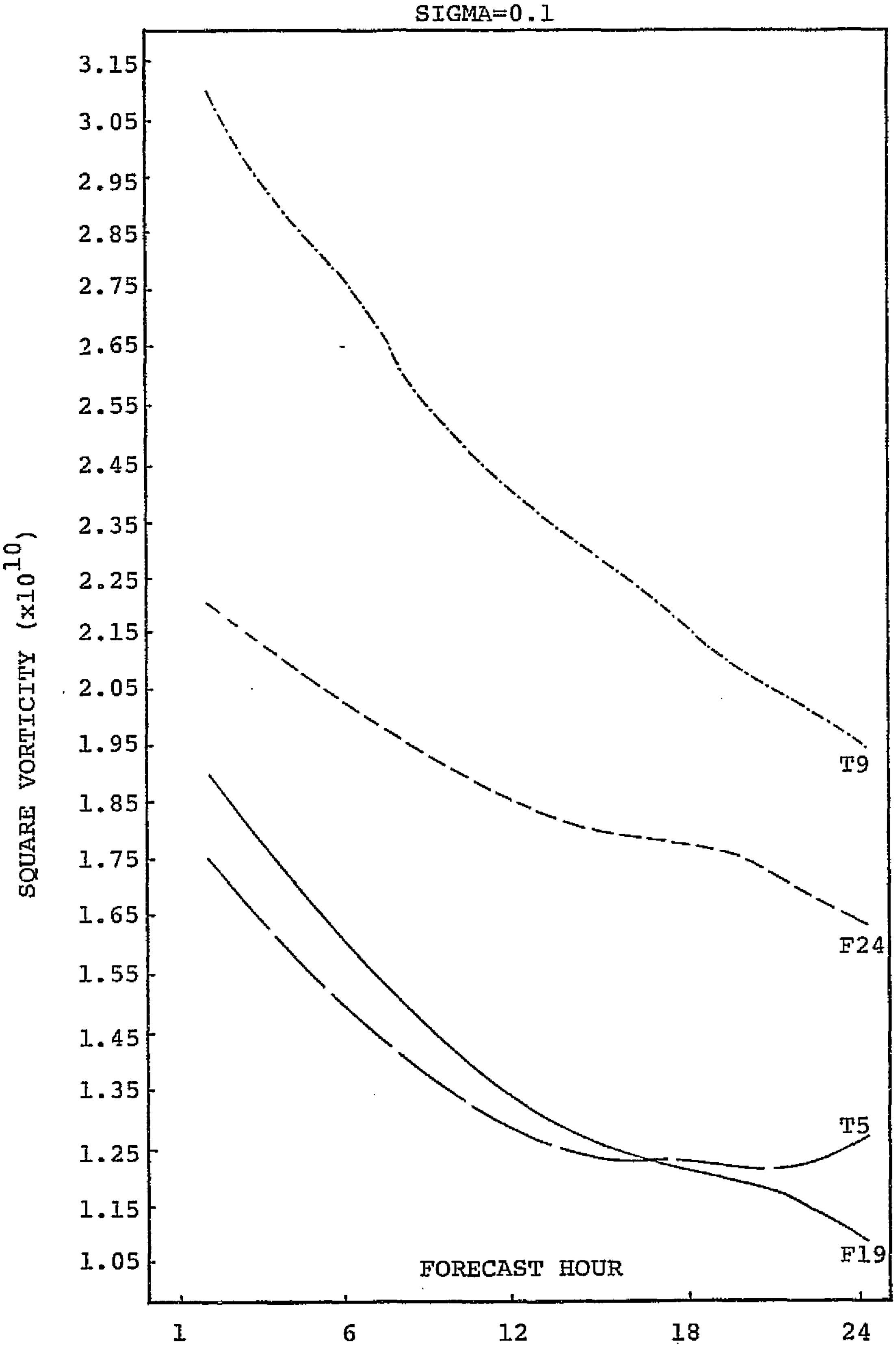

FIGURE VII-16: TIME VARIATION OF SQUARE VORTICITY FOR FOUR MODEL VERSIONS AT SIGMA=0.1 LEVEL. SCENARIO B.

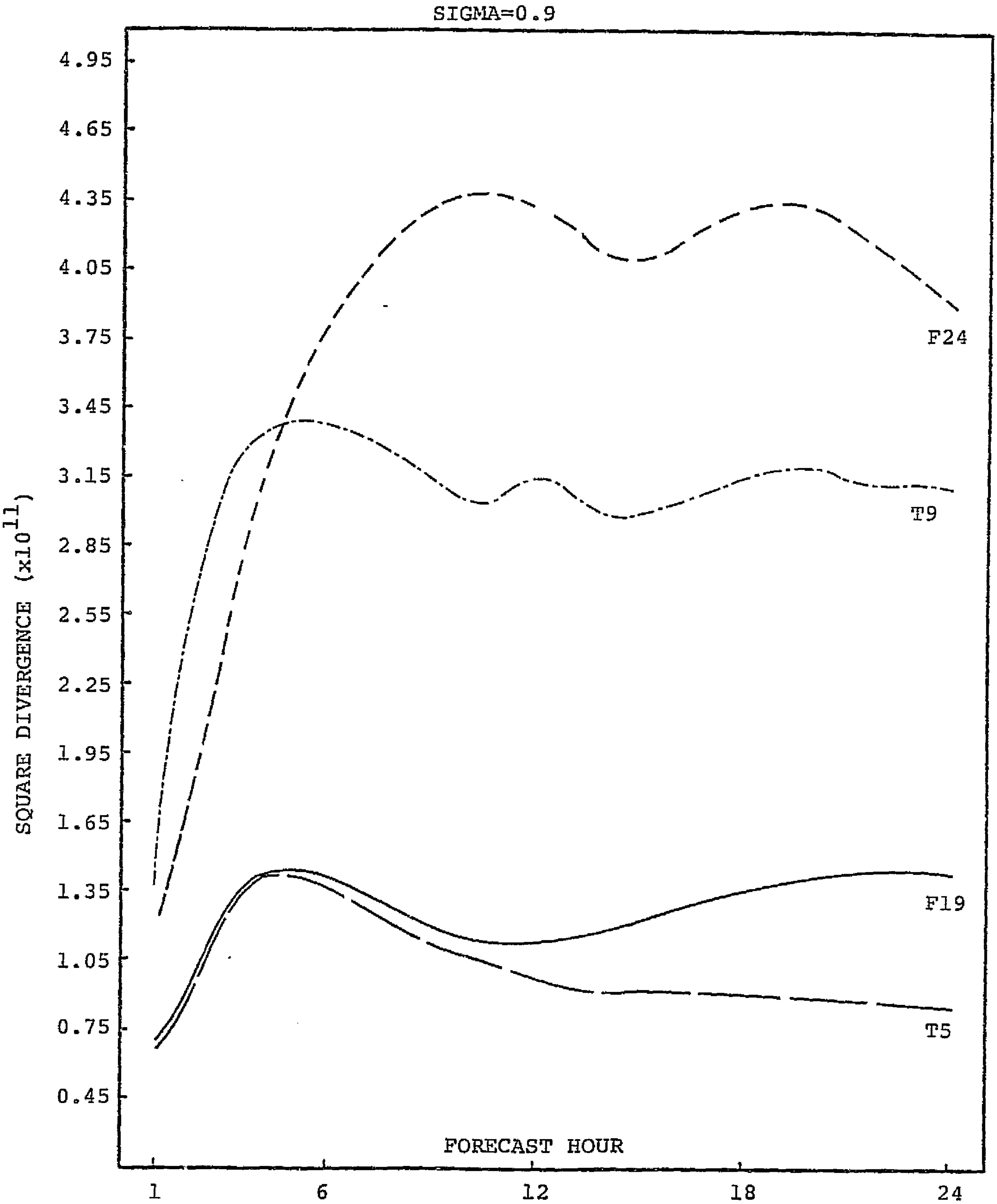

FIGURE VII-17: TIME VARIATION OF SQUARE DIVERGENCE FOR FOUR MODEL VERSIONS AT SIGMA=0.9 LEVEL. SCENARIO B.

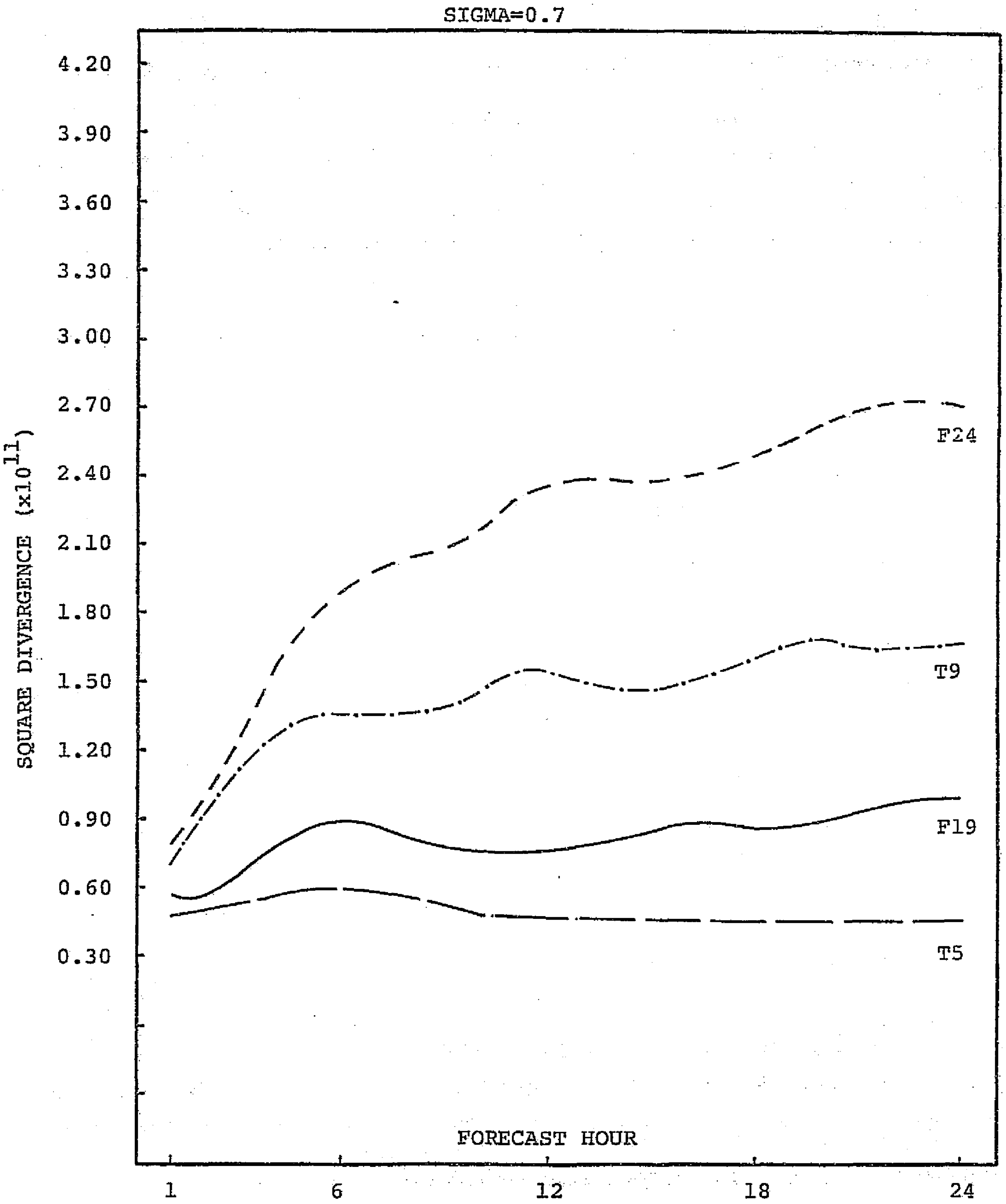

FIGURE VII-18: TIME VARIATION OF SQUARE DIVERGENCE FOR FOUR MODEL VERSIONS AT SIGMA=0.7 LEVEL. SCENARIO B.

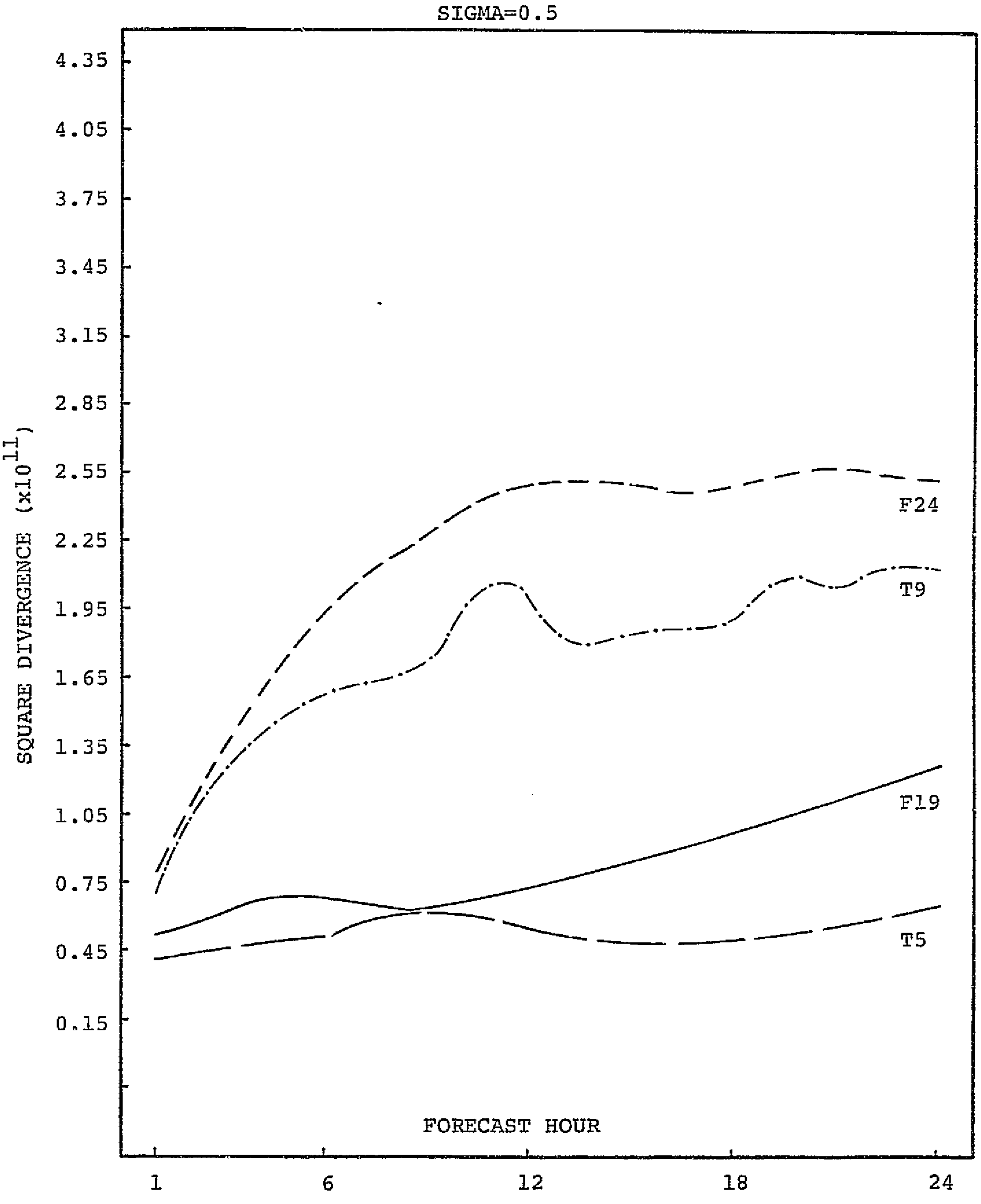

FIGURE VII-19: TIME VARIATION OF SQUARE DIVERGENCE FOR FOUR MODEL VERSIONS AT SIGMA=0.5 LEVEL. SCENARIO B.

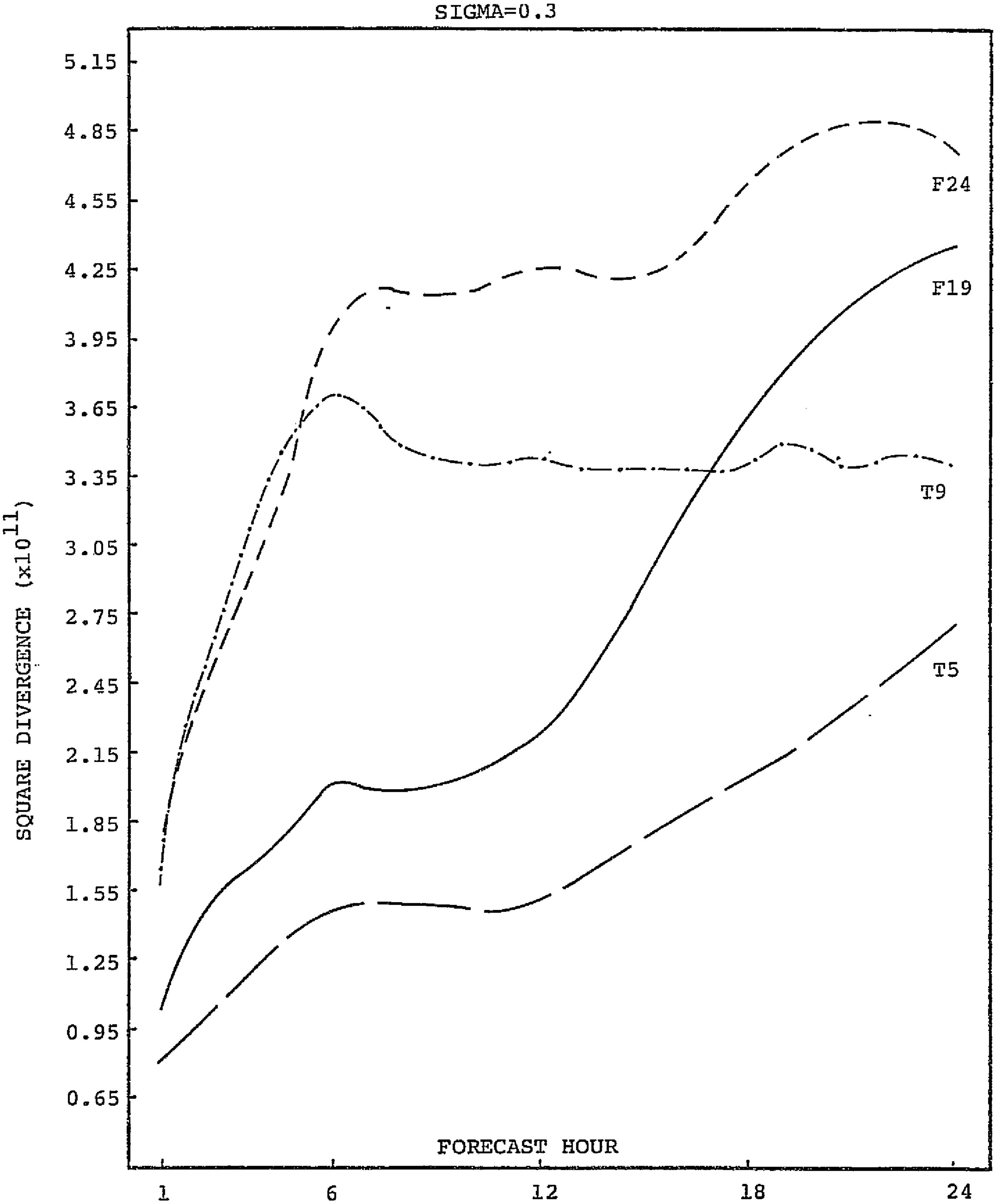

FIGURE VII-20: TIME VARIATION OF SQUARE DIVERGENCE FOR FOUR MODEL VERSIONS AT SIGMA=0.3 LEVEL. SCENARIO B.

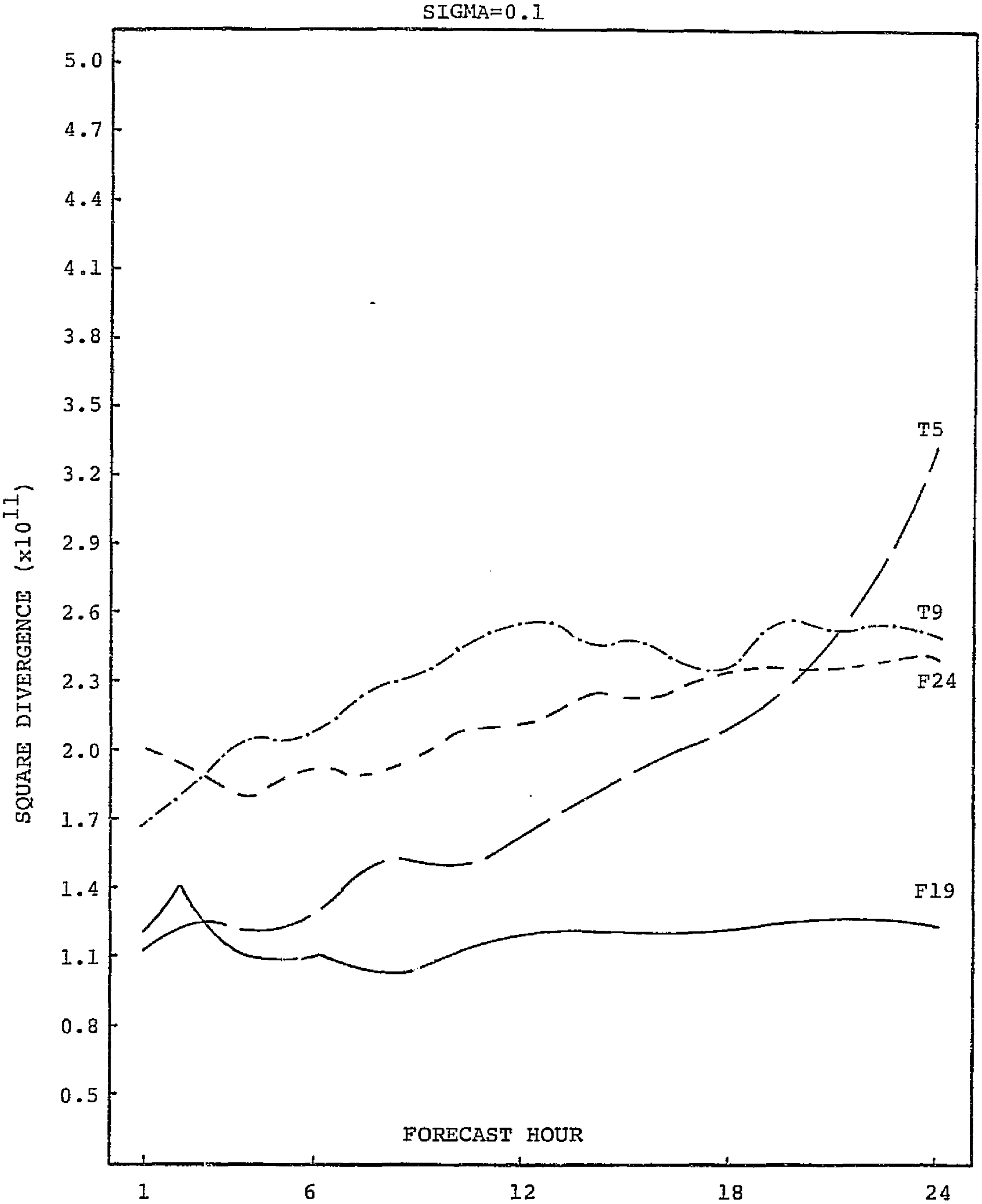

FIGURE VII-21: TIME VARIATION OF SQUARE DIVERGENCE FOR FOUR MODEL VERSIONS AT SIGMA=0.1 LEVEL. SCENARIO B.

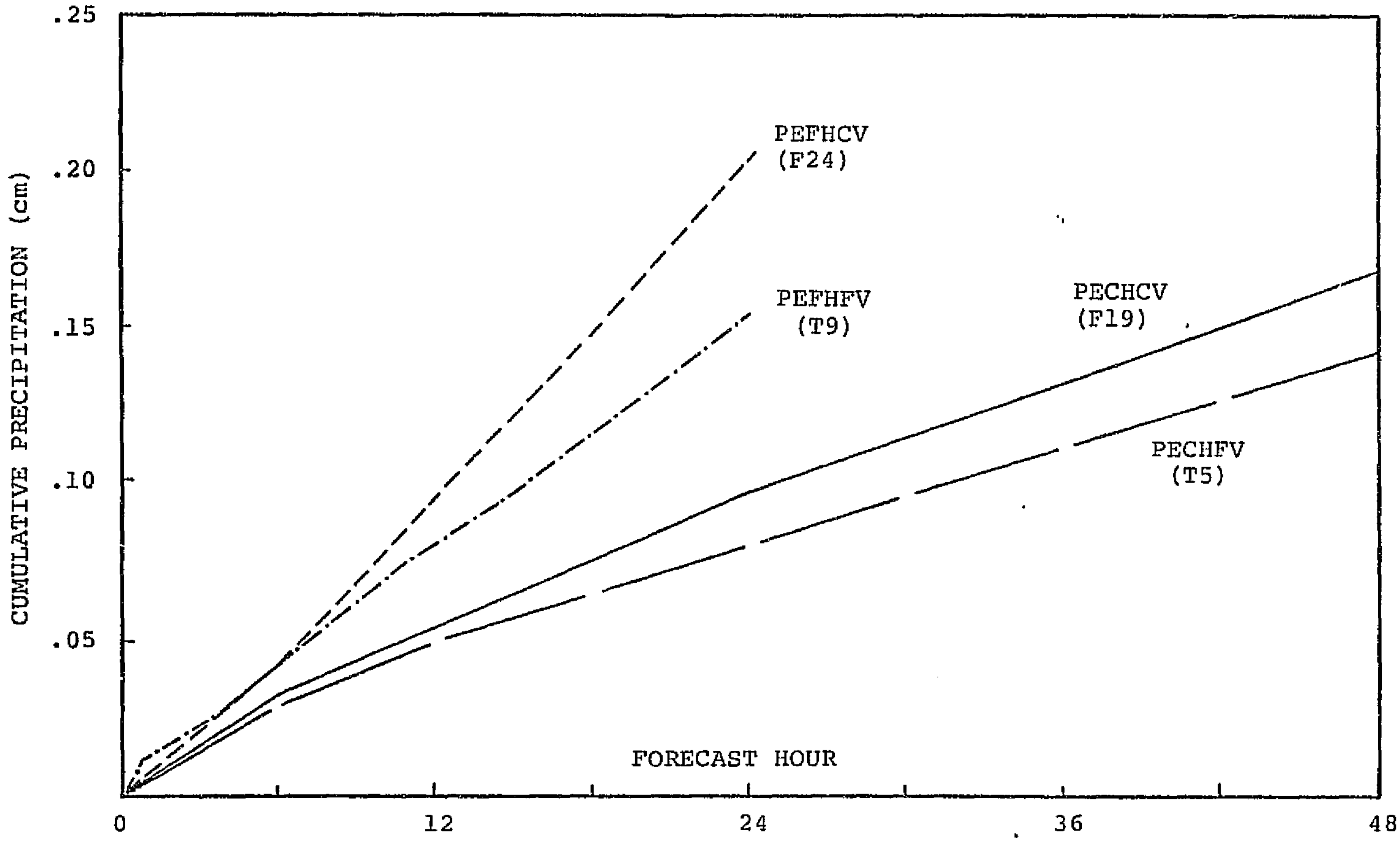

FIGURE VII-22: PRECIPITATION (PER GRID POINT) FOR FOUR MODEL VERSIONS. SCENARIO B.